# Uplift Resistance of an Under-Reamed Piled Foundation

**by**

**Daniel Harris (CHR)**

**Fourth-year undergraduate project**

**In Group D, 2013/2014**

***"I hereby declare that, except where specifically indicated, the work submitted herein is my own original work."***

**Signed:** **Date:**

# Technical Abstract

Structures require that the loads upon them can be transmitted to the ground safely. Although, these loads are usually compressive in nature, under certain conditions, upward tensile forces can exist which the foundation must be designed to cope with. One method of dealing with this phenomenon is through the use of under-reamed piles: piled foundations with an enlarged base cross section designed specifically to resist uplift forces.

At present, experimental studies and literature has focused on the uplift piles with flat anchor plates attached to the base, known more commonly as plate anchors. Almost no previous literature considers or analyses the effects of varying the under-reaming angle on the pile behavioural characteristics, such as ultimate uplift capacity or displacement to failure.

For this research project, a series of 1g tests were conducted to characterise the effect the under-reaming angle has upon the various load characteristics of the pile. The tests were conducted using dry sand in both loose and dense states. Two primary sets of tests were conducted. The first consisted of rounds of standard pullout tests using fully formed model aluminium piles to measure the load-displacement behaviour. The second test series used particle image velocimetry (PIV) and half space pile models to characterise the failure mechanism for these piles in uplift, with primary focus on the influence of sand density and under-reaming angle on the mechanism characteristics. The aim of the experiments was to carry out a comparative study between different under-ream angles in order to determine the effect varying this parameter has upon the ultimate uplift capacity, load-displacement behaviour of the pile, and the failure mechanisms geometrical form. The results were also compared to an existing theoretical model (Meyerhof & Adams 1968) for uplift capacity of plate anchors and existing literature on the failure mechanism geometry.

It was found that the uplift capacity of under-reamed piles in loose sand decreases as the under-reaming angle increases. In dense sand the relation is more complex, with an optimum under-reaming angle being observed to approximately coincide with 45° - φ/2 that would give an optimum uplift capacity. The stiffness of the pile response was found to increase with the sand relative density, with the failure displacement being much lower for dense sands relative to loose sands. Instability in the form of soil arching was observed to initiate post failure, commencing at greater displacements for plate anchors than cases where the under-

reaming angle was greater than zero. The displacement that this behaviour initiated was observed to be unaffected by sand density.

The PIV tests on the plate anchor and 45 degree pile under-ream found that uplift failure mechanism changed with both the sand density and the under-reaming angle. The plate anchor failure mechanism in dense sand closely matched that described in previous literature. However, the mechanism for the plate anchor in loose sand was found to differ from theoretical predictions, with the pile exhibiting a deep pile failure mechanism contrasting to the predicted shallow mechanism as observed for the dense sand case. The under-reaming angle was found to have a noticeable effect on the mechanism close to the pile base, but significantly less influence on the mechanism geometry away from this region. The results from the PIV tests matched those from the 1g pullout tests, and explained the under-ream angle relationships observed.

The theory presented in Meyerhof & Adams (1968) for determining the ultimate uplift capacity of a plate anchor was found to generally over predict the experimental uplift resistance for all under-reamed angles, with the degree of over-estimation being greater in loose sand. The errors found for the dense sand case were determined to relate to the assumptions made in deriving the uplift capacity equation in the Meyerhof model, specifically for the term modelling the frictional resistance of the sand. Adjusting the assumed failure mechanism to the observed mechanism in the PIV experiments for the loose case was found to predict capacities around 25-30% lower than observed. Adjusted shape factors were proposed to correct this.

More experiments need to be carried out to follow on from the work conducted in this paper, due to the lack of existing literature in this field and 1-g nature of the tests conducted in this study. Particular areas that would provide further insight into the problem would be to investigate the effect of the pile-soil interface friction angle on the piles behaviour, particularly the failure mechanism geometry local to the pile base, and the load-displacement response of various under-reaming angles in large scale model or centrifuge tests, to see whether the relationships found here carry over to pile geometries and scales expected to be used in practice. Lastly, it would be of great value to carry out the similar tests in clays to determine the corresponding pile behaviour in such soils.

# Acknowledgements

I would like to acknowledge and thank Professor Gopal Madabhushi for his help and supervision throughout the project. I would also like to acknowledge the Schofield Centre technicians for their support and aid in constructing parts of my experimental apparatus and technical advice concerning my experimental procedure. Lastly, I would like to thank both Dr Charles Heron and Peter Kirkwood for their assistance in teaching me the particle image velocimetry methodology and aiding me with general queries throughout the projects duration.

# Table of Contents

# Nomenclature

| | |
|---|---|
| Δ | Pile head displacement [m] |
| A | Average inclination angle of the passive earth pressure acting on a vertical plane through the edge of the pile base [°] |
| Δ | Interface angle of friction between the pile and the soil [°] |
| $\theta$ | Pile under-ream angle measured from the horizontal [°] |
| $\tau_f$ | Average shear stress mobilised on the failure surface [N/m$^2$] |
| $\varphi_{crit}$ | Critical state internal soil friction angle [°] |
| $\varphi_{max}$ | Maximum internal soil friction angle [°] |
| $\varphi_{mod}$ | Modified maximum internal soil friction angle [°] |
| $\Psi$ | Soil dilation angle during shearing [°] |
| B | Pile base diameter [m] |
| D | Embedment depth of pile measured from the soil surface to the bottom of the pile base or point of widest diameter (the datum level) [m] |
| H | Vertical extent of the failure surface above the datum level [m] |
| $K_p$ | Coefficient of passive earth pressure [-] |
| W | Weight of pile base and shaft [N] |
| F | Mobilised friction force on the failure surface [N] |
| $N_{qu}$ | Dimensionless breakout factor [-] |
| $Q_u$ | Ultimate uplift capacity [N] |

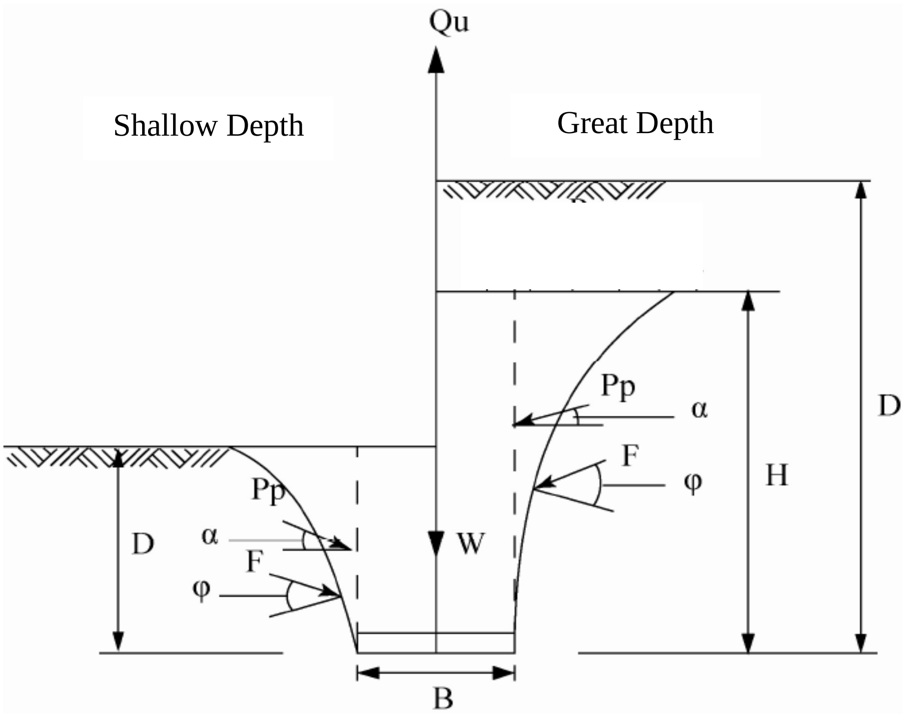


**Figure (i): Failure Surface of a plate anchor under uplift load (from Meyerhof & Adams (1968))**

# 1 Introduction

## 1.1 Background

In order for structures to support themselves, they exert loads on the ground through the use of footings or foundations. Under certain loading conditions, these loads can be tensile and hence the foundation exerts an uplift force on the soil around it. There are a number of situations in which this can occur, a common scenario being lightweight steel frame buildings or structures (e.g. electrical pylons,) where high lateral wind loading creates large overturning moments at the foundation level. This coupled with the low self weight of the structure, causes tensile forces that the windward foundations must be able to transmit into the soil.

**Figure 1: Black Cotton Soil is highly moisture retentive, and can undergo large volumetric strains upon seasonal changes. In order to isolate structures from these large ground deformations, uplift resisting piles are used (civil-engg-world.blogspot.co.uk/ (2012))**

Historically, large gravity based foundation systems have been used for foundations subject to large overturning moments, but more modern methods have demonstrated piled schemes to be more economical, both in cost and material usage for such loading scenarios. For such schemes, select piles need to be designed to resist uplift forces. Sites with expansive soils, such as "Black Cotton Soil" (commonly found in India) require similar uplift foundations. Black Cotton Soil experiences large volumetric strains when subject to the substantial moisture variations between monsoon seasons, which can lead to large surface deformations. In order to isolate the structure from this, uplift piles with under-reamed bases are typically used to provide the necessary anchorage force, but at a lower depth, where soil deformations are smaller.

## 1.2 Under-Reamed Piles

Under-reamed piles are a type of pile with a mechanically formed enlarged base, designed to increase the capacity of the pile. The base geometry is typically in the form of an inverted cone. This enlarged base can be used to either increase the compressive base capacity, or provide uplift resistance by forcing a passive failure wedge of soil to mobilize for failure to occur. They are classically bored piles, with the enlarged base being constructed via use of a rotary cutting tool.

## 1.3 Motivation for Work

In order to design foundations for tensile forces, the mathematics behind the uplift resistance of soil must be understood. Currently, the theory behind the uplift resistance of plate anchors is relatively well understood, but that of under-reamed piles is not due to lack of academic research, despite being used in industry in certain circumstances. Thus, the primary aim for this project was to make headway in understanding the effect of varying the under-ream angle upon the load-displacement characteristics and performance of piles in uplift.

## 1.4 Problem Definition

This research follows on directly from the work conducted by Hopkins (2012), and will examine the uplift capacity and load-displacement response of a number of under-reamed piles under 1g condition in small scale tests, both in loose and dense dry sand. Model aluminium alloy piles will be used. Additionally, this research will characterise the failure mechanism and investigate its variation with the pile under-reaming angle, testing half space models of both a plate anchor and 45 degree under-reamed pile at small scale, again in both loose and dense sands. This research will form a comparative study between different under-ream angles but will not aim to predict load response or settlement for fully sized piles. This research will use dry, homogeneous sand stratum for testing and investigation.

## 1.5 Project Objectives

This project will aim to:

- Compare the uplift capacity and load-displacement relationship of a range of under-ream angles, with a fixed pile base and diameter, in both loose and dense sand, using standard pullout tests.
- Characterise the uplift failure mechanism using particle image velocimetry (PIV) for plate anchors and under-reamed piles in loose and dense sand, investigating the effect varying the under-ream angle has upon the mechanism geometry.
- Review and discuss the analytical methods present in existing literature on the uplift capacity of such piles, comparing the experimental results to existing theoretical models, evaluating their accuracy as relevant to small scale testing.

# 2 Literature Review

There is a substantial amount of existing literature that has been published investigating the uplift behaviour of plate anchors, but a lack of research concerning the more general under-reamed pile case. Only Balla (1961) has considered under-reamed piles as of writing this report, with other investigations approximating the under-reamed case as a plate anchor. The following papers discussed in this section are those most relevant to the experimental work undertaken in this project.

## 2.1 Ultimate Uplift Capacity

Research into the uplift capacity of foundations began in earnest in the early 1960's, notably commencing with Balla (1961)'s investigation into the uplift resistance of "mushroomed" piles for transmission towers. Meyerhof & Adams (1968) proposed a theoretical model for the problem, where they examined the uplift capacity of plate anchors in lab experiments and available field test data. They found that the problem was a complex one, with many relevant variables, but simplified the problem to develop a generalized theory for predicting the uplift capacity of plate anchors. They distinguished between two categories of behaviour: where the failure mechanism extends to the surface and where it does not, which they defined as "shallow" and "deep" foundations respectively.

Geddes & Murray (1987) evaluated pre-existing literature on uplift in cohesionless soils and used limit state approaches to compute upper and lower bounds for a plate anchor's uplift capacity in said soils. They established that the theory using Kotter's equations used by Khadilkar et al. (1971) and others was invalid due to the ignoring of normal stresses on the failure surface which meant the solution did not satisfy equilibrium. They presented the uplift capacity in terms of a normalised resistance: $N = \frac{Q_u}{\gamma' A H}$, a notation which has been predominant in future literature. From their experiments, they found a good agreement with Meyerhof & Adams (1968) for dense sands, but found the model to over predict capacity for looser sands.

Dickin (1988) investigated the uplift behaviour of horizontal plate anchors, using 1g and centrifuge testing. His results compared well with the predictions of Meyerhof & Adams, but noted a discrepancy between the 1-g and centrifuge test results, where extrapolation from the former to the latter produced over-estimates of capacity. The same observation was made by Oveson (1979). Both papers noted instability occurring post failure for the anchors, with significant oscillations in load occurring at large displacements.

Ilamparuthi et al. (2002) investigated the transition between shallow and deep anchor behaviour. They found that the relationship between displacement at peak load and embedment ratio was bi-linear, changing gradients at a critical value, which allowed the distinction between shallow and deep behaviour to be specified. These results coincided well with the critical embedment depths published by Meyerhof & Adams (1968).

Merrifield & Sloan (2006) conducted a numerical study using the plasticity bound theorems and finite element modelling, as opposed to traditional finite element methods, comparing their solutions to numerical databases and empirical solutions from existing literature. Their analysis was restricted to plane strain geometry and so has limited applicability to the problem of circular plate anchors. They found a large dependence of the soil-pile interface friction angle, with this dependence lessening in magnitude for very dense sands with high internal friction angles. However, their results did not compare well with those of Geddes & Murray (1987), indicating that the latter may be unconservative by up to 30% if adopting their methodology. In addition, no critical embedment was detected in contrast to Ilamparuthi (2002) and Meyerhof & Adams (1968) indicating their results' applicability for large embedment depths may be questionable.

Bolton et al. (2008) investigated and compared the various underlying methodologies for computing uplift capacity. Although only considering the plane strain, they determined plasticity solutions to be inappropriate in the analysis of drained soil problems. It was concluded that the limit equilibrium approach to be valid, provided the relevant parameters such as soil effective unit weight, relative density, embedment depth and confining stress could be computed accurately. Methods using the plasticity theorems were shown to be invalid for dry sands because the normality rule, and underlying assumption for the theorems, is not observed in such drained condition tests.

Hopkins (2012) investigated the uplift capacity and load-displacement relationship for plate anchors and under-reamed piles in homogeneous sand stratum using 1g small scale tests. He found that the load displacement data trend for all under-ream angles matched closely to that expected from standard shear box testing of sand, with dense sand showing initial dilatory behaviour with a peak capacity, before reaching a critical state, and loose sand showing contractile behaviour with no peak strength being shown above critical state. He found that there was a relationship between a piles uplift capacity and its under-ream angle, but did not investigate further. He did however note that for large under-ream angles (approaching 75 degrees) a transition in mechanism occurred which caused a large drop in capacity and as such, large under-ream angles should be avoided. He also observed the post failure instability noted by Dickin (1988) and Oveson (1979).

## 2.2 Failure Mechanism Characterisation

Throughout the literature, various failure surface mechanisms have been assumed for plate anchor pullout, but extremely little research has been conducted on the influence of variation in under-ream angle from this specific case. Meyerhof & Adams (1968) noted that the lack of agreement with regards to a unifying uplift resistance theory arose from difficulties in characterising the failure mechanism geometry, a view also shared by Geddes & Murray (1987). Ilamparuthi et al. (2002) carried out semi-large scale experiments on the uplift capacity of cylindrical plate anchors using half space models to observe the soil during failure. They also conducted an extensive literature review on the previously proposed failure mechanism geometries. 3 main mechanism types were highlighted for shallow anchors:

- Vertical Slip Surface Model (VSSM) – i.e. a cylindrical failure surface projected up above the piles base area. Ilamparuthi et al (2002) found this surface geometry to be conservative for shallow embedments but not so for deep embedments.
- Truncated Soil Cone Model – a cone model extending out at an angle θ from the footing edge. Similar to the VSSM, this geometry was found to be conservative for shallow embedment's but not so for deep embedment's.
- Circular Arc Model – circular arc failure surface as seen in figure 2c. Initially proposed by Balla (1961) but also observed by Baker & Konder (1966).

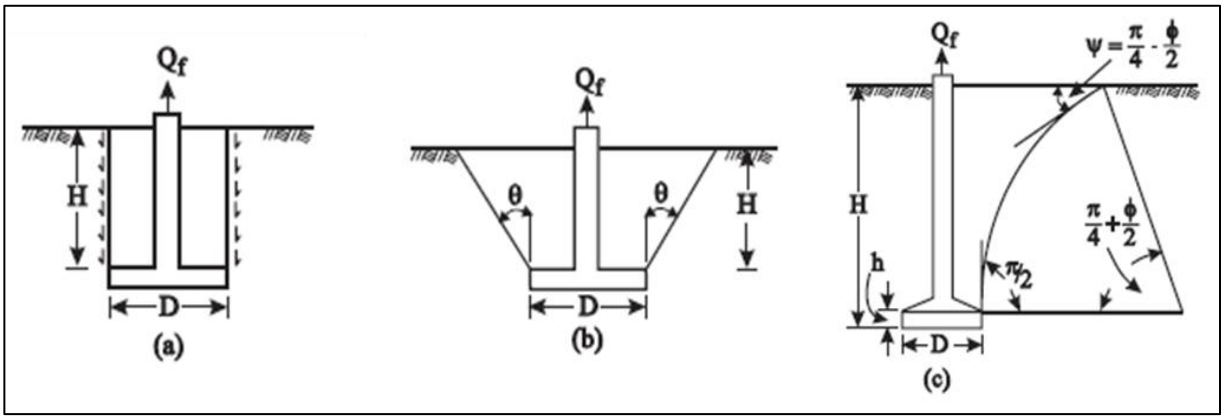


**Figure 2: Assumed Failure Surfaces: (a) vertical slip surface model, (b), soil cone model, and (c) circular arc model (Ilamparuthi et al. (2002))**

The different failure surfaces are illustrated above in figure 2. For deep anchors, the failure surface characterisation has not been researched in depth, but Ilamparuthi et al. (2002) found that a smooth “balloon shaped” mechanism symmetrical about the anchor axis, was typical from their half space model tests.

Dickin (1988) investigated the accuracy of the VSSM, and also found it to be highly conservative. Curved failure surfaces such as that in figure 2c have also been considered, notably by Geddes & Murray (1987). Although such a curved surface was initially considered for their limit equilibrium analysis, a final equation for a truncated soil cone mechanism was found. They found that a value for the angle $\theta = \varphi$ (where $\varphi$ is the mobilised soil friction angle,) provided a conservative upper bound for shallow anchors, with $\theta = \varphi/2$ providing a better average capacity estimation. Since then, this value for $\theta$ has been reduced to approximately $\varphi/2$, with half space models from Ilamparuthi et al. (2002) finding that $\theta$ could be approximated by $\varphi/2 \pm 2°$: $\varphi/2 - 2°$ for relatively loose sands, and $\varphi/2 + 2°$ for relatively dense sands.

## 2.3 Soil Friction Angle and Dilatancy

Bolton (1986) proposed how to calculate the peak friction angle in sand for use when dilatants behaviour is expected. The tests conducted for this research are 1-g small scale tests. Thus the confining pressure within the soil will be significantly lower than true piles in the field would experience. To account for this alteration, Drescher & Detourney (1993) proposed a modified friction angle to use (exact formulae covered in section 4.2). This method has been corroborated by Davis (1968 and Michalowski (1997). This method requires calculation of the angle of dilation of the soil. Schanz & Vermeer (1996) proposed an analytical expression for calculating this angle following on from Bolton (1986).

## 2.4 Summary

The experiments and theoretical model proposed by Meyerhof & Adams (1968) have been shown to provide a useful method for predicting uplift capacity of plate anchors. This approach, combined with the widely accepted dilatancy of sand model initially proposed by Bolton (1986) with friction angle adjustments proposed by Drescher & Detourney (1993) will be used to compare the experimental results in the research presented in this report, in a similar manner to that used by Hopkins (2012). The truncated cone failure mechanism highlighted by Ilamparuthi et al (2002) has been widely validated for large scale shallow plate anchor tests and hence will also be compared with the results from this research.

# 3 Experimental Equipment and Methodology

Two types of test were carried out: standard pullout tests that measured the load-displacement response of the pile, and PIV experiments using half space models to characterise the failure mechanism. This section details the experimental method, setup procedure, test rigs used and any notable points concerning the work conducted or data processing.

## 3.1 Test Containers

### 3.1.1 Pullout test container

The pullout tests were performed in a cylindrical steel container with 850mm diameter and 400mm depth. The edges had pre-drilled holes to allow for installation of the pile jig at various orientations. The container was chosen to ensure the container edges did not interfere with the mechanism and affect the results. Moreover, the container size allowed 3 piles to be tested per experiment which increased testing efficiency over smaller tubs.

### 3.1.2 PIV experiment container & control marker layout

The PIV tests were performed in a timber container, 705mm long, 300mm wide and 500mm deep, with the front face being a detachable, clear perspex window. The tubs size was large enough to prevent the container edges affecting the results, provided each pile was to be tested individually, with a new sand pour being conducted each time.

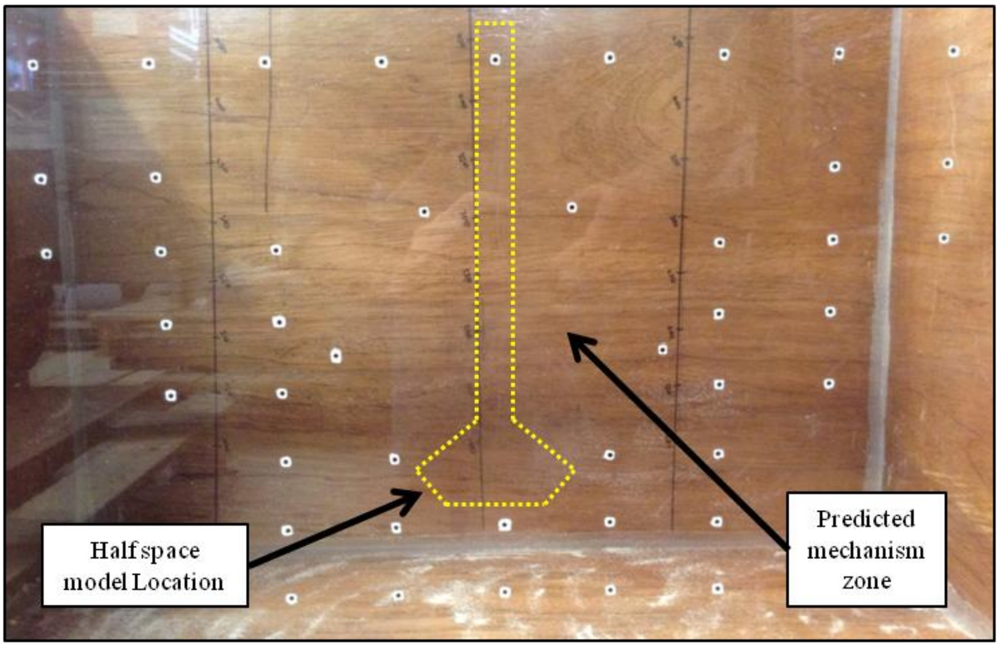


**Figure 3: PIV Control Marker Layout**

Figure 3 shows the PIV control marker layout used. The layout ensured the minimum 14 markers required for the PIV software would be safely met, and minimised the number of markers that would overlay the mechanism, ensuring shear bands would not be obstructed, with the mechanism being captured as fully as possible. Two markers remained within the predicted mechanism zone to maintain accurate calibration in that area. The layout assumed a conical mechanism, being the predominant agreed upon geometry from the literature review.

## 3.2 Soil Used

All tests were performed in dry Hostun HN31 sand. Hostun HN31 is a uniform, easy to handle and readily available sand at the Schofield Centre, and hence was used for the experimental work. Sand was used instead of clay for a couple of reasons:

- Time constraints imposed on 4$^{th}$ year projects limited the number of tests that could be carried out. Testing in sand meant that experimental models were much quicker to prepare and hence more tests could be conducted to gather repeat data.
- Installation of the piles was simpler in sand and required less apparatus to hold the piles in place whilst the model was being prepped.

Properties for HN31 sand were taken from multiple sources and are presented in table 1. The parameter values determined by Mitrani (2006) and Haskell (2013) were used because they were determined for the same Hostun sand in the same laboratory, and hence were more likely to reflect the sand being used in this study.

**Table 1: Properties of Hostun HN31 sand, taken from multiple sources**

| | Mitrani (2006) | Flavigny (1990) | Haskell (2013) |
|---|---|---|---|
| $e_{min}$ | 0.555 | 0.648 | - |
| $e_{max}$ | 1.01 | 1.041 | - |
| $\varphi_{crit}$ | - | - | 33° |

## 3.3 Model Piles, Anchors and Under-Reams

The model piles and under-reams were machined from blocks of Dural aluminium alloy and were 400mm in length and 12.7mm in diameter, with the under-ream geometry being as shown in figure 4. Under-reams with angles of θ equivalent to 20°, 30°, 45°, 60° and 75° were used in addition to a plate anchor or identical diameter and 4.5 mm thickness. These models were the same as those used by Hopkins (2012), with the exception of the 20° under-ream, which was manufactured for this research in order to better fill out the range of experimental data collected. The small size of the expected pile loads meant that movement of the whole pile was much larger than any deformations occurring within it. Hence, extensions due to strains in the pile shaft were ignored and the pile bases were modelled as perfectly rigid.

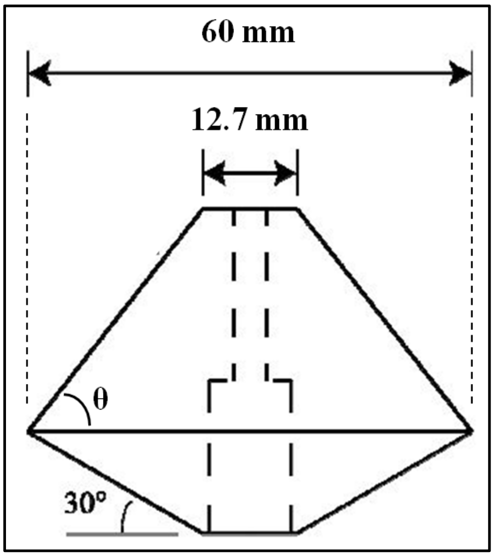


**Figure 4: Model under-ream base geometry**

Two half space models for the PIV tests were also constructed, with the cross section geometry as shown in figure 4. Half space models of the plate anchor and 45° under-ream were built, with a layer of PTFE tape attached to the flat face to provide a low friction interface with the perspex window. This was to allow accurate comparison of the load-test data recovered in these tests to the full 3D pullout tests. A rectangular cross section for the shafts was selected as it was much easier to manufacture than a semi-circular cross section.

**Figure 5: A selection of the model under-reamed piles, with both half space models shown on the far right.**

## 3.4 Actuator

A 1-D actuator was used to apply a constant rate of displacement to the top of the pile shaft in order to supply the uplift force. A shear box was used to control the rate of displacement, with a constant rate of 0.1mm/s being adopted across all tests. This rate was constant to ensure the rate of application of load was not a variable within the analysis, and the low value of 0.1mm/s was chosen to ensure no dynamic effects were present, and any settlement of the sand had time to occur during the test run.

## 3.5 Instrumentation and Measurement

### 3.5.1 Load measurement

Load measurement was carried out using an 800 N load cell, which was placed between the actuator and the pile head. To calibrate the load cell, the pile was replaced by a hanger, onto which successive weights were carefully added with the output voltage being recorded. The load cell was calibrated before and after each test to ensure data consistency across the project. Calibration equipment and a typical calibration curve are shown in figure 6. The type of load cell used was very sensitive to applied moments, so measures to ensure the load transmitted into it was purely axial were adopted. For calibration, this entailed using pin connectors, shown in figure 6a.

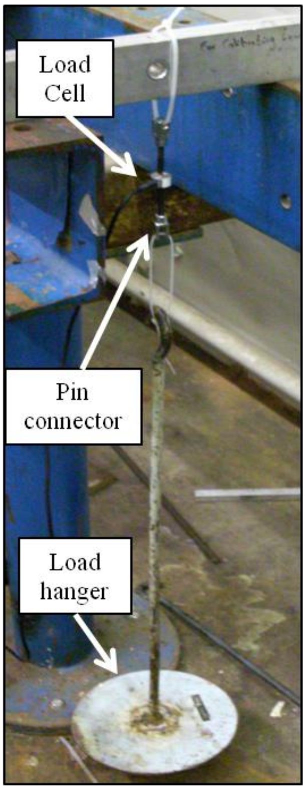


(a)

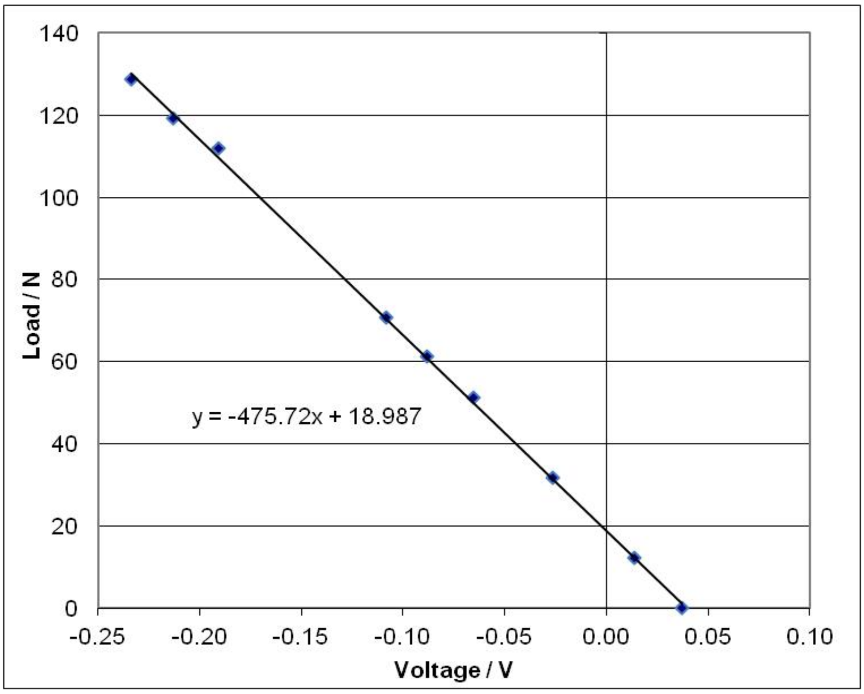


(b)

**Figure 6: (a) Load cell calibration apparatus and (b) a typical load cell calibration curve**

### 3.5.2 Displacement measurement

The pile head displacement was measured using a Linear Variable Differential Transformer (LVDT), which was calibrated in a corresponding manner to the load cell. During experiments, the LVDT was placed above the actuator carriage so as to measure using a flat surface. Both instruments produced a voltage output that varied linearly with the measured variable. At the extreme ends of the LVDT's travel, this linearity broke down, and so measures were taken to maintain an experimental operating point away from these regions. DASYlab data logging software was used to record the data continuously from both instruments.

## 3.6 Experimental Setup

### 3.6.1 Pullout test jig and pile securing

**Figure 7: Pullout test jig, securing the piles in place during sand pouring and vibro compaction.**

A jig was manufactured for the purpose of holding the piles in position during the model preparation for the pullout tests (includes pile positioning and sand pouring.) As mentioned in section 3.5.1, the load cells were very sensitive to applied moments, and thus this jig was designed to guarantee the piles were installed vertically and not on an incline. The jig also held the piles in place whilst the sand was compacted between loose and dense sand tests. This sped up testing time significantly as only one sand pour per test round was required instead of two. Figure 7 shows the jig in question. Due to the container geometry, a jig was impractical for the PIV test preparation so instead, a plum bob, masking tape and a D-clamp allowed the pile to be aligned and secured in place. The tape was then removed sequentially during sand pouring.

### 3.6.2 Sand pouring

In order to create a homogeneous sand stratum, the relative density had to be controlled carefully during the sand pour. A manual hopper was used for sand pouring. Test pours gave hopper settings that would correspond with the desired "loose" and "dense" relative densities. A loose density of $I_d \approx 0.2$, and a dense density of $I_d \approx 0.6 - 0.65$ were decided upon to use throughout the project. Practical limitations on the pouring process meant that relative densities above 70% were not achievable via the manual hopper, but values of 65% were achievable both with the hopper and vibration table, hence the values adopted. In order to achieve these relative densities in a uniform manner over the containers, an oscillatory pouring pattern was adopted, as demonstrated in figure 8.

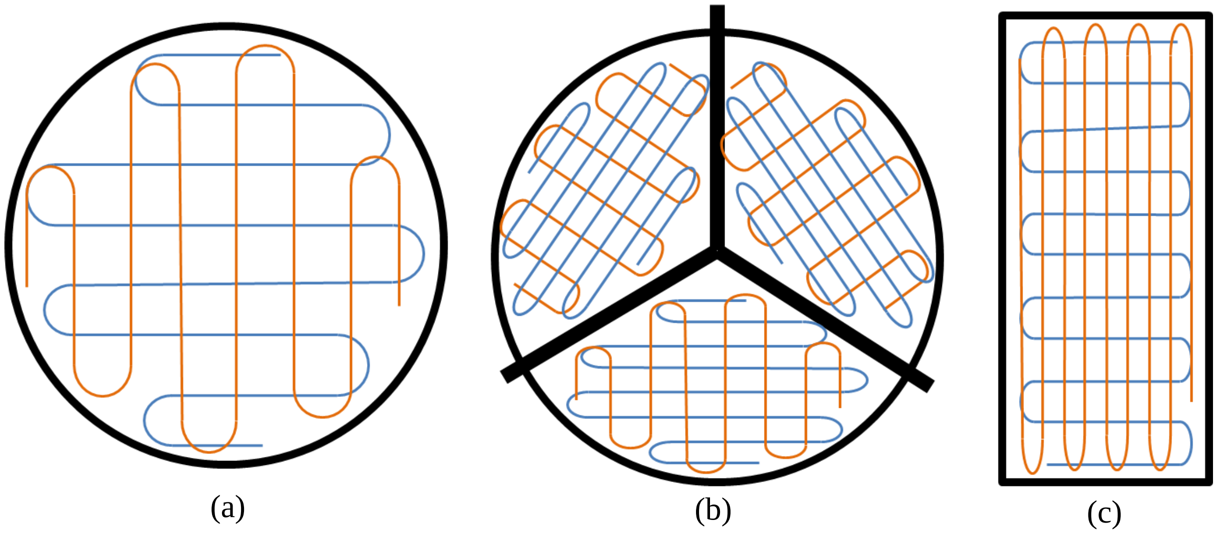


**Figure 8: Sand pouring patterns for (a) initial layer in circular tub, (b) once the jig and piles were in place and (c) the PIV tests**

An initial 100mm layer of sand was poured for both the pullout and PIV tests to rest the pile bases onto. Following this, the piles were positioned and secured (see section 3.6.1), after which the pour recommenced using a similar pouring pattern (also shown in figure 8), taking care to manoeuvre around the jig without knocking the piles. Once the required mass of sand had been poured, the surface was levelled and the pile embedment depths recorded. For each pour, the mass of sand added and the final sand depth was recorded in order to calculate the achieved relative density.

### 3.6.3 Sand compaction (pullout tests)

To save time and increase the number of pullout tests that could be carried out, a loose pour was done first, the piles were then tested, and then the sand was vibro compacted in situ with the piles held in place. This allowed the dense sand test for the 3 piles to be conducted on the same day, without needing to fully prepare the model from scratch. The aforementioned jig (section 3.6.1) was used to hold the piles in place during this process, and the sand was compacted via placing the container on a vibrating table until the surface sand level had decreased by the desired amount.

### 3.6.4 Full experimental setup

The complete experimental setup for both types of test is shown in figure 9.

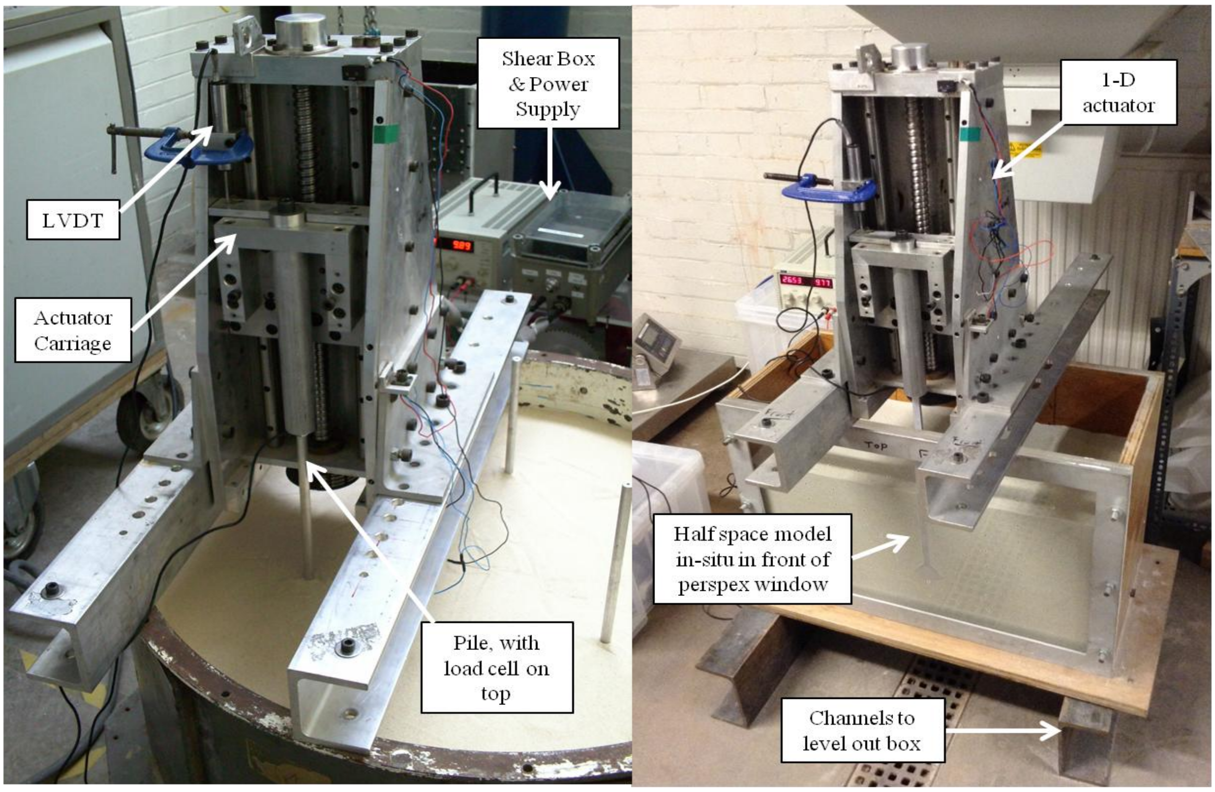


**Figure 9: Experimental setup. Left = pullout test arrangement. Right = PIV test arrangement**

## 3.7 PIV Specifics: blue sand, sand ingress and data processing notes

Blue HN31 sand was mixed with standard HN31 in a 1:10 ratio. This was done to increase the texture of the sand surface up against the perspex window, hence increasing the amount of texture in the images fed into the PIV code and decrease the likelihood of wild vectors (tracking failures) occurring in the data processing stage. An issue noticed during preparation of the first test was that sand would slip in-between the pile and perspex window during model preparation. This needed to be avoided to provide accurate PIV results, and so the following prevention measures were adopted: a coat of silicon grease was applied to the PTFE tape on the flat pile face. This grease was low friction so as to not affect the pile capacity significantly, and provided a seal/ barrier that prevented sand ingress.

The camera used was a GoPro HERO 3+ Black edition. For the experiments, a 4k resolution video was shot of the deformation mechanism. This was then converted into a series of 4k image stills, which were the image the sand particles were tracked over. The PIV patch size and spacing finally used were 24x24 pixels at a 24 pixel spacing. This patch size successfully tracked the sand and gave results at a good resolution, where shear bands could be detected at sufficient detail. It was deemed to be the best compromise between computational processing time and resolution. Moreover, smaller patches were tested and gave substantially more wild vectors and hence were not selected.

## 3.8 Experimental Procedure

### 3.8.1 Pullout test procedure

All pullout tests were conducted using the following procedure:

1) Set hopper up correctly and pour the initial 100mm sand layer into the container.
2) Fix jig into place and position piles, ensuring they are vertical using a spirit level.
3) Pour remaining sand, recording the sand added as you go.
4) Level the sand surface and record the final height.
5) Remove jig, place actuator over pile, using a plum bob to gauge the correct position. Attach the load cell, LVDT and check all electrical equipment is recording correctly.
6) Set shear box and power supply to correct settings, start DASYlab recording and apply the set displacement rate to the pile. Continue recording data until failure.
7) Detach and move actuator and all instruments, and move onto the next pile.
8) Once all piles have been tested, move container onto vibrating table. Compact sand. Conduct the dense sand pile tests for each pile, using the same procedure as before.
9) Remove sand and clean tub to prepare for next test.

### 3.8.2 PIV test procedure

The PIV test procedure was similar to that in 3.7.1, but instead of using the jig, the half space model was secured up against the perspex using the methodology described in 3.6.1, the rig only held 1 pile instead of 3, and a new sand pour was conducted for each test – no compaction was carried out. The 100mm initial sand layer was still used.

## 3.9 Experimental Accuracy

The nature of the PIV tests meant that adopting the measures described in 3.7 ensured good quality, useable data. The pullout tests however were harder to ensure accuracy in, with the relevant issues being to ensure the piles were vertical (see section 3.6.1) and getting accuracy out of the load cell data. The load cell was the primary concern for accuracy due to its sensitivity to applied moment loading as previously highlighted. To negate this in experiments, the connection between the pile head, load cell and the actuator cylinder (shown in figure 9) was assembled carefully, ensuring the actuator was placed flat onto the test container and aligned exactly with the pile head beforehand. In addition, metal rings were placed on the load cell screws to allow the connection to be fully tightened effectively and remove all give from the connection before load transfer occurred.

## 3.10 Tests Performed

Table 2a details the pullout tests performed. These tests were conducted in the Michaelmass academic term and used fully formed model piles as detailed previously.

**Table 2a: Details of the standard pullout tests performed**

| Name | Aim of Test | Relative Density $I_D$ | Under-Ream Angle [°] | D / B |
|---|---|---|---|---|
| **DH-1a** | To compare the resistance of piles with various under-reaming angles in loose sand. | 0.16 | 0<br>45<br>75 | 3.50<br>3.50<br>3.50 |
| **DH-1b** | To compare the resistance of piles with various under-reaming angles in dense sand. | 0.58 | 0<br>45<br>75 | 3.00<br>2.93<br>2.90 |
| **DH-2a** | To compare the resistance of piles with various other under-reaming angles in loose sand. | 0.21 | 30<br>45<br>60 | 3.50<br>3.50<br>3.50 |
| **DH-2b** | To compare the resistance of piles with various other under-reaming angles in dense sand. | 0.64 | 30<br>45<br>60 | 3.01<br>3.03<br>2.98 |
| **DH-3a** | To provide pullout test data for a 20° under-ream and get repeat data points to fill out the data for loose sand. | 0.17 | 0<br>20<br>75 | 3.50<br>3.50<br>3.50 |
| **DH-3b** | To provide pullout test data for a 20° under-ream and get repeat data points to fill out the data for dense sand. | 0.57 | 0<br>20<br>75 | 3.00<br>3.14<br>3.00 |
| **DH-4a** | To carry out control tests for a number of under-reamed bases in loose sand. | 0.17 | 0<br>30<br>60 | 3.50<br>3.50<br>3.50 |
| **DH-4b** | To carry out control tests for a number of under-reamed bases in dense sand. | 0.60 | 0<br>30<br>60 | 2.95<br>2.89<br>2.98 |

Table 2b details the PIV tests performed. These tests were conducted in the Lent academic term and used half space model piles as also detailed previously.

**Table 2b: Details of the PIV tests performed**

| Name | Aim of Test | Relative Density $I_D$ | Under-Ream Angle [°] | D / B |
|---|---|---|---|---|
| **DH-PIV-1a** | To determine the failure mechanism for a plate anchor in loose sand. | 0.22 | 0 | 3.33 |
| **DH-PIV-1b** | To determine the failure mechanism for a plate anchor in dense sand. | 0.60 | 0 | 3.25 |
| **DH-PIV-2a** | To determine the failure mechanism for a 45° under-reamed pile in loose sand. | 0.21 | 45 | 3.25 |
| **DH-PIV-2b** | To determine the failure mechanism for a 45° under-reamed pile in dense sand. | 0.66 | 45 | 3.25 |

# 4 Theoretical Models Used

This section details the uplift resistance model detailed in Meyerhof & Adams (1968) that will be used to compare the test results. Additionally, required adjustments to soil parameters due to the 1g nature of the experiments are covered.

## 4.1 Meyerhof & Adams Model of Uplift Resistance

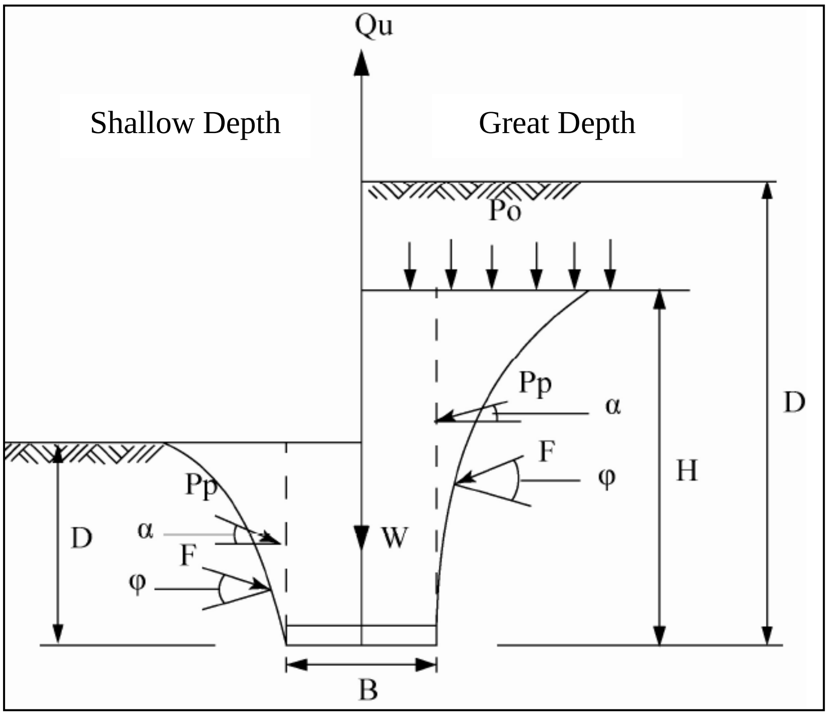


**Figure 10: Failure Surface of a plate anchor under uplift load (from Meyerhof & Adams (1968))**

Meyerhof & Adams (1968) proposed a theoretical model for the evaluation of the uplift capacity of plate anchors, based on the friction of a projected soil cylinder above the pile base. The parameter definitions are provided graphically in figure 10. The first principles derivation is for plain strain geometry, with adjustment factors to convert the problem for use with circular base geometries, as is standard in modern geotechnical design. The derivation below is that provided in Meyerhof & Adams (1968), but has all terms relating to cohesion removed, as dry sand (the soil tested in this research), is cohesionless.

The model distinguishes between anchors at shallow depth and those at great depth via whether the failure mechanism extends to the soil surface, where it does for the former, but not the latter. The extent of the mechanism (denoted 'H') can only be determined from the observed failure surface. Estimates of the critical embedment depths, where if $D/B > (H/B)_{critical}$, then the anchor behaves as if it's as great depth, are shown in table 3.

**Table 3: Critical values for H/B in terms of φ**

| Friction Angle φ | 20° | 25° | 30° | 35° | 40° | 45° | 48° |
|---|---|---|---|---|---|---|---|
| Critical Depth H/B | 2.5 | 3 | 4 | 5 | 7 | 9 | 11 |

For this research, linear interpolation was used within this table to determine which mechanism form the model predicted and hence the theoretical uplift capacity.

For a footing at shallow depth, the shear stress mobilized at failure may be written as

$$\tau_f = \sigma \tan(\varphi) \tag{4.1}$$

where σ is the normal stress on the failure surface, and φ is the internal soil friction angle. The ultimate load per unit length of a footing may then be expressed as

$$Q_u = 2F\cos(\beta) + W \tag{4.2}$$

where W is the total mass of the pile and lifted soil, and β is the average angle with the vertical of force F over the entire failure surface. In the absence of a rigorous solution for the stresses on the failure surface, one can assume the uplift capacity may be approximated by

$$Q_u = 2P_p\sin(\delta) + W \tag{4.3}$$

where $P_p$ is the total passive earth pressure inclined at an average angle δ acting downwards on a vertical plane through the edge of the footing. Expressing the normal component of $P_p$

$$P_p\cos(\delta) = \gamma(\frac{D^2}{2})K_p \tag{4.4}$$

where γ is the soil unit weight and $K_p$ is the passive earth pressure coefficient. Substituting (4.4) into (4.3)

$$Q_u = \gamma D^2 K_{pv} + W \tag{4.5}$$

where $K_{pv} = K_p \tan(\delta)$. Trial calculations from Meyerhof & Adams (1968) have shown that δ can accurately be approximated as 2φ/3. For uplift under these assumptions, the corresponding passive earth pressures may be written as $K_p = K_u$ where $K_u$ = the nominal uplift coefficient of earth pressure on a vertical lane through the footing edge. The value of $K_{pv}$ may thus be evaluated as shown in figure 11. The polynomial curve fit for $K_u$ displayed in figure 10 was used in the analysis to aid in construction of a calculation spreadsheet.

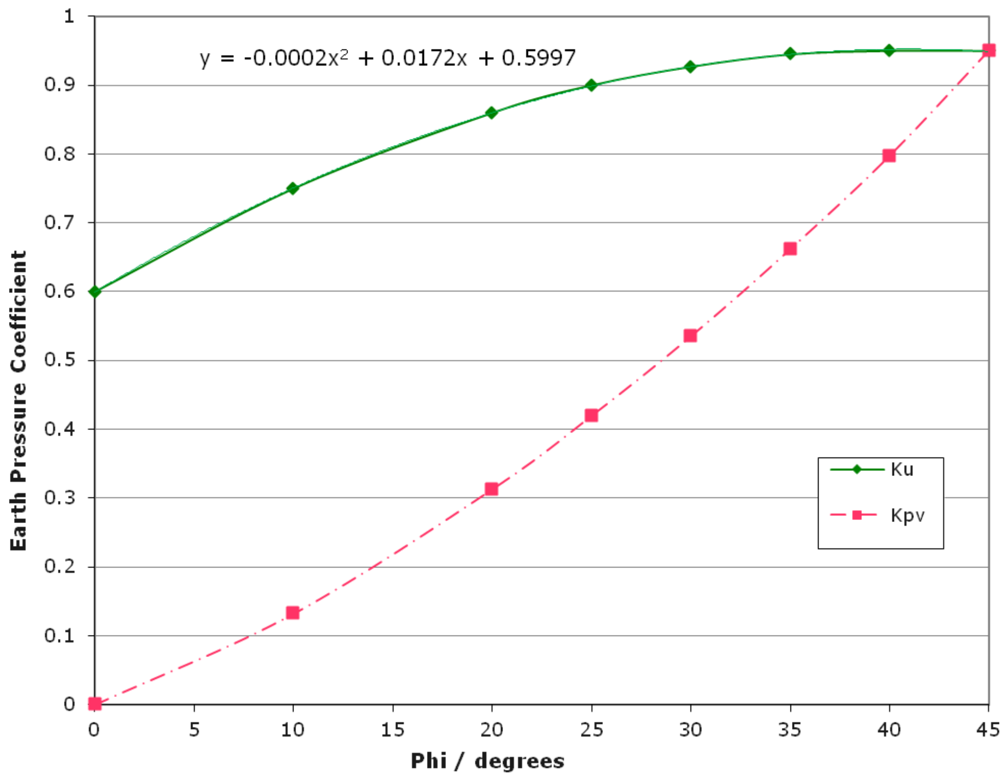


**Figure 11: Coefficients of passive earth pressures (Meyerhof & Adams (1968))**

Substituting in for $K_{pv}$, equation (4.5) becomes

$$Q_u = \gamma D^2 K_u \tan(\varphi) + W \tag{4.6}$$

Now for a footing at great depth as distinguished using table 3, the extent of the local shear failure will be limited to the value H. Utilising the surcharge pressure above the failure surface level of $P_o = \gamma(D\text{-}H)$, equation (4.6) becomes

$$Q_u = \gamma(2D - H)HK_u \tan(\varphi) + W \tag{4.7}$$

Equations (4.6) and (4.7) can then be modified for a circular footing by determining the shearing resistance on a vertical cylindrical surface through the footing edge. For shallow depths (i.e. D<H), adopting this procedure means equation (4.6) becomes

$$Q_u = s\frac{\pi}{2}\gamma BD^2 K_u \tan(\varphi) + W \tag{4.8}$$

and for great depths, equation (4.7) becomes

$$Q_u = s\frac{\pi}{2}\gamma B(2D - H)HK_u \tan(\varphi) + W \tag{4.9}$$

where *s* is the shape factor governing the passive earth pressure on a convex cylindrical wall. For small values of D/B, the quantity s can be approximated by:

$$s = 1 + m\frac{\min[D,H]}{B} \tag{4.10}$$

where D<H for a footing at shallow depth and vice versa for a footing at great depth. The co-efficient *m* has values given in table 4 below. Using these equations, a theoretical uplift capacity for an anchor plate can be computed, which can be compared to experimental results.

**Table 4: Values of m and maximum value of s for the uplift of circular anchor plates**

| Friction Angle φ | 20° | 25° | 30° | 35° | 40° | 45° | 48° |
|---|---|---|---|---|---|---|---|
| Coefficient "m" | 0.05 | 0.10 | 0.15 | 0.25 | 0.45 | 0.50 | 0.60 |
| Maximum "s" Value | 1.12 | 1.30 | 1.60 | 2.25 | 3.45 | 5.50 | 7.60 |

## 4.2 Determination of the Soil Friction Angle φ

The soil friction angle used in equations (4.1) to (4.10) must be determined in order for the uplift capacity to be evaluated. This is done using a combination of Bolton's stress Dilatancy (Bolton (1986)) and a modified friction angle approach. Loose soils subject to shear deformation exhibit contractile behaviour, with the soil friction angle approaching the critical value of $\varphi_{crit}$, at which no volumetric change occurs upon further shearing. For loose sand tests in this project, a friction angle of $\varphi = \varphi_{crit}$ was used. In contrast, for dense soils, the initial behaviour is dilatants, with a peak friction angle being observed (denoted $\varphi_{max}$) where $\varphi_{max} > \varphi_{crit}$. Bolton (1986) proposed a now widely accepted method for accounting for the dilatancy of sands and calculating $\varphi_{max}$, which will now be described.

First, the relative Dilatancy is defined as:

$$I_R = I_d I_c - 1 \tag{4.11}$$

where $I_d$ is the relative density and $I_c$ is the relative crushability as defined below:

$$I_d = \frac{e_{max} - e}{e_{max} - e_{min}} \tag{4.12}$$

$$I_c = \ln\frac{\sigma_c}{p'} \tag{4.13}$$

where p’ is the mean confining stress at that location and $\sigma_c$ is the aggregate crushing stress. For HN31 sand, $\sigma_c$ is taken to be 20000 kPa. Bolton’s peak friction correlation then states that for axisymmetric strain conditions:

$$(\varphi_{max} - \varphi_{crit}) = 3^\circ * I_R \tag{4.14}$$

The tests conducted for this project were small scale tests conducted at 1g and hence the confining stress in the soil is very small, thus the increase in friction angle is predicted to be very large using Bolton’s stress dilatancy method and overestimates the effective friction angle. Consequently, as stated in section 2, a modified friction angle for low confining stresses is calculated as proposed by Davis (1968), Drescher & Detourney (1993) and Michalowski (1997), using the relation

$$\tan(\varphi_{mod}) = \frac{\cos(\psi)\sin(\varphi_{max})}{1 - \sin(\psi)\sin(\varphi_{max})} \tag{4.15}$$

Where $\varphi_{mod}$ is the modified friction angle and $\psi$ is the dilation angle. In order to predict the dilation angle, Schanz & Vermeer (1996) proposed the following relation:

$$\sin(\psi) = \frac{I_R}{6.7 + I_R} \tag{4.16}$$

Combining equations (4.11) to (4.16), the soil friction angle may be calculated and used in the formulae presented by Meyerhof to predict the uplift capacity of a plate anchor.

## 4.3 Failure Mechanism Form used in Predictions

From equations (4.8) and (4.9), we can see that the uplift capacity of a plate anchor has two terms: a term relating to the shear stress mobilized on the failure surface and a term for the weight of the pile itself and the soil mass lifted. Although the first is hard to change without conducting a fully involved first principles analysis, similar to that conducted by Meyerhof & Adams (1968), the latter is trivial to adjust depending on what failure mechanism geometry is predicted. In sections 5 and 6, a comparison is made between the results using the truncated cone surface and VSSM as highlighted in Ilamparuthi et al (2002). For each geometry, the weight of soil mass term is altered, and the shear stress term will have simply be adjusted between the shallow and deep pile variants shown in equations (4.8) and (4.9) where relevant. The algebraic form of this shear stress term will not be altered as the purpose in this report is to evaluate, not change the model. This data will be used to compare the accuracy of Meyerhof’s method when used with different assumed mechanisms.

# 5 Pile Performance: Load-Displacement Results

In this section, the results from the pullout tests are presented and discussed. The load-displacement curves are plotted on normalised axes to coincide with previous literature on this subject. The results are compared, first with each other to determine what effect under-reaming angle has on the load characteristics of the pile, and then to existing theory, with the load capacity being evaluated using the Meyerhof and Adams method detailed in section 4.

## 5.1 Observed Load-Displacement Curves

### 5.1.1 Comparison between loose and dense sand

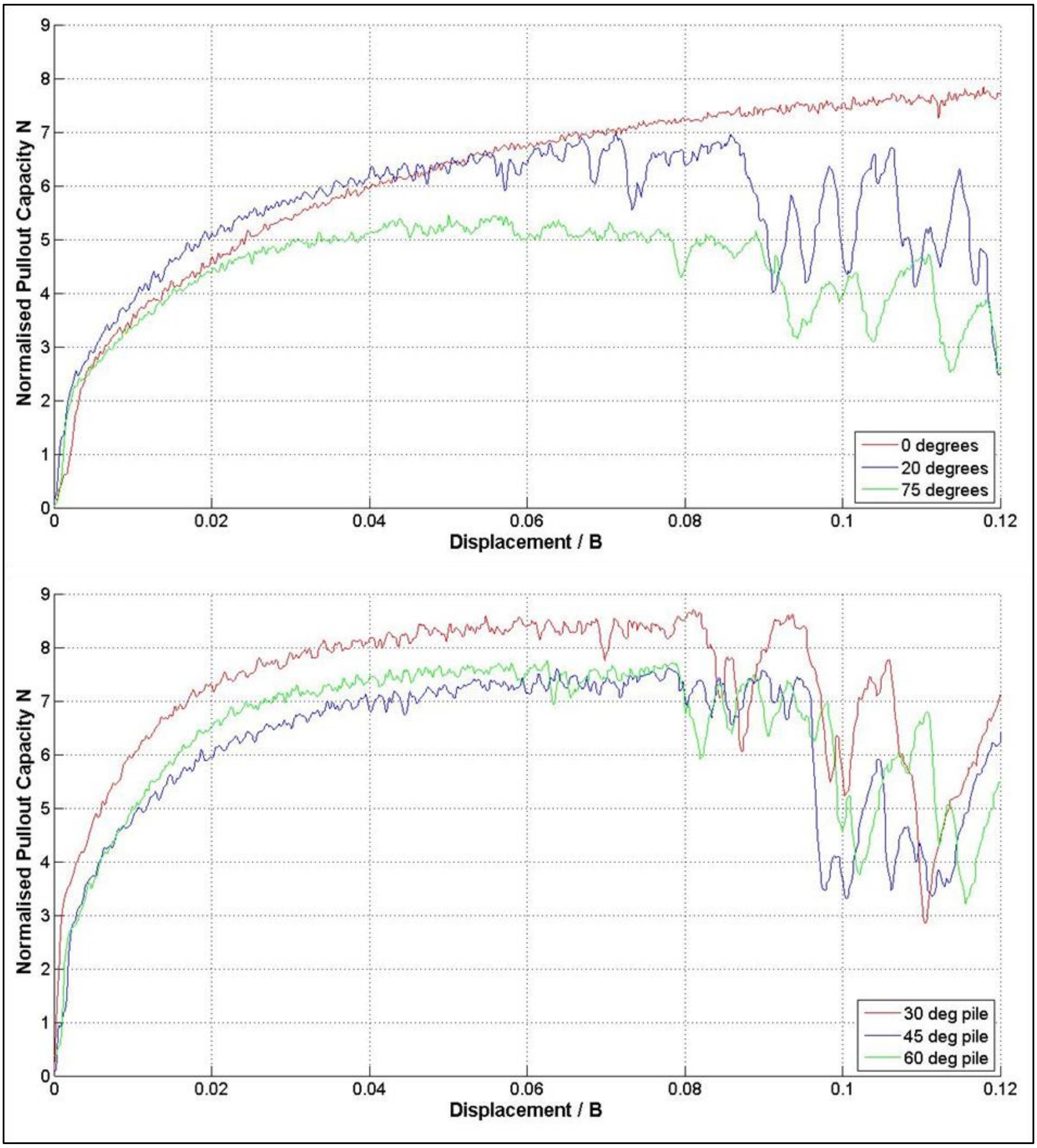


**Figure 12: Non-dimensionalised load displacement curves for under-reamed piles in loose sand.**

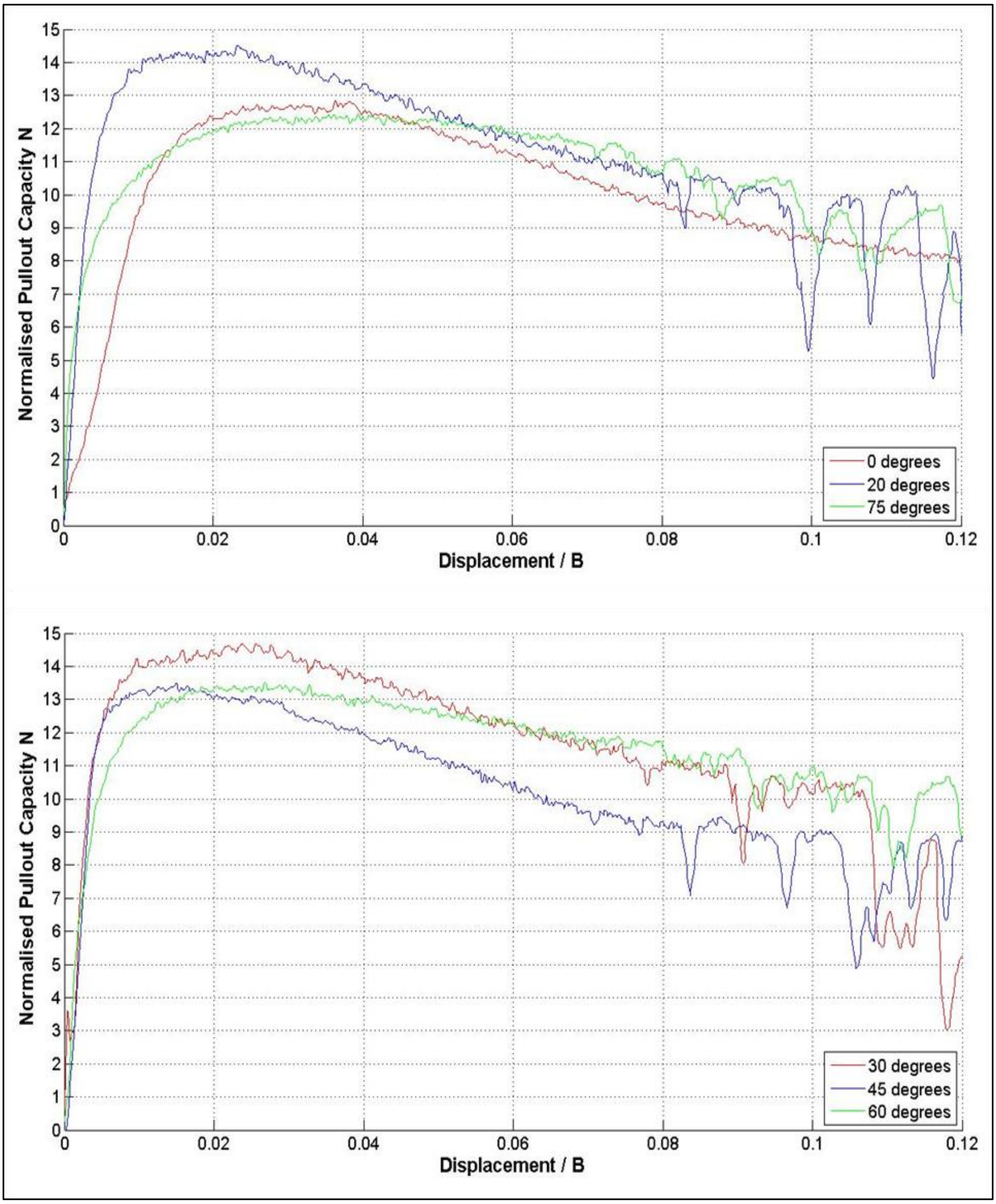


**Figure 13: Non-dimensionalised load displacement curves for under-reamed piles in dense sand.**

Figures 12 and 13 show non-dimensionalised load-displacement curves for various under-reamed piles in loose and dense sand respectively, as taken from tests DH-2 and DH-3. As can be seen from these two figures, the curve forms are similar across all the under-ream angles tested. In addition, the curve forms closely follow the expected behaviour of sand when subjected to a direct shear stress. The loose sand tests showing contractile behaviour and tending to a critical state at large displacements, where further shearing occurs at constant volume and the dense sand tests exhibit initial dilatory behaviour, reaching a peak strength at relatively low displacement, followed by post peak softening down towards a critical state. This trend was also found by Hopkins (2012) but does not agree with the results of Ilamparuthi et al. (2002) which are discussed in section 5.2.1.

Additionally, from figures 12 and 13 it can be seen that the initial stiffness of the piles in dense sand is much greater overall than those in loose sand. Although the stiffness of the piles is approximately constant across both sand density designations tested and all under-ream angles whilst the soil undergoes very small shear strains ($\delta/B < 0.004$), this behavioural trend breaks down beyond N values of approximately 3 this breaks down as the loose sand response's secant stiffness begins to drop. This leads to an overall much stiffer initial response in the dense sand case, as is expected and seen in many other areas of geotechnical engineering.

Both figures also show that the capacity for all under-reamed piles is shown in be significant greater for the dense sand than the loose sand. Hence it is shown that pile uplift capacity increases with sand density, as logically expected. Hopkins (2012) noted in his study that for dense sand, the dilatant peak became much narrower and more pointed in form for larger under-ream angles, with the plate anchor experiencing gradual post peak softening as further displacement occurred and under-reamed piles experiencing much faster softening. This trend is not seen in figure 13, with no apparent relation being observed, contrasting to Hopkins's observation.

### 5.1.2 Displacement to failure trends

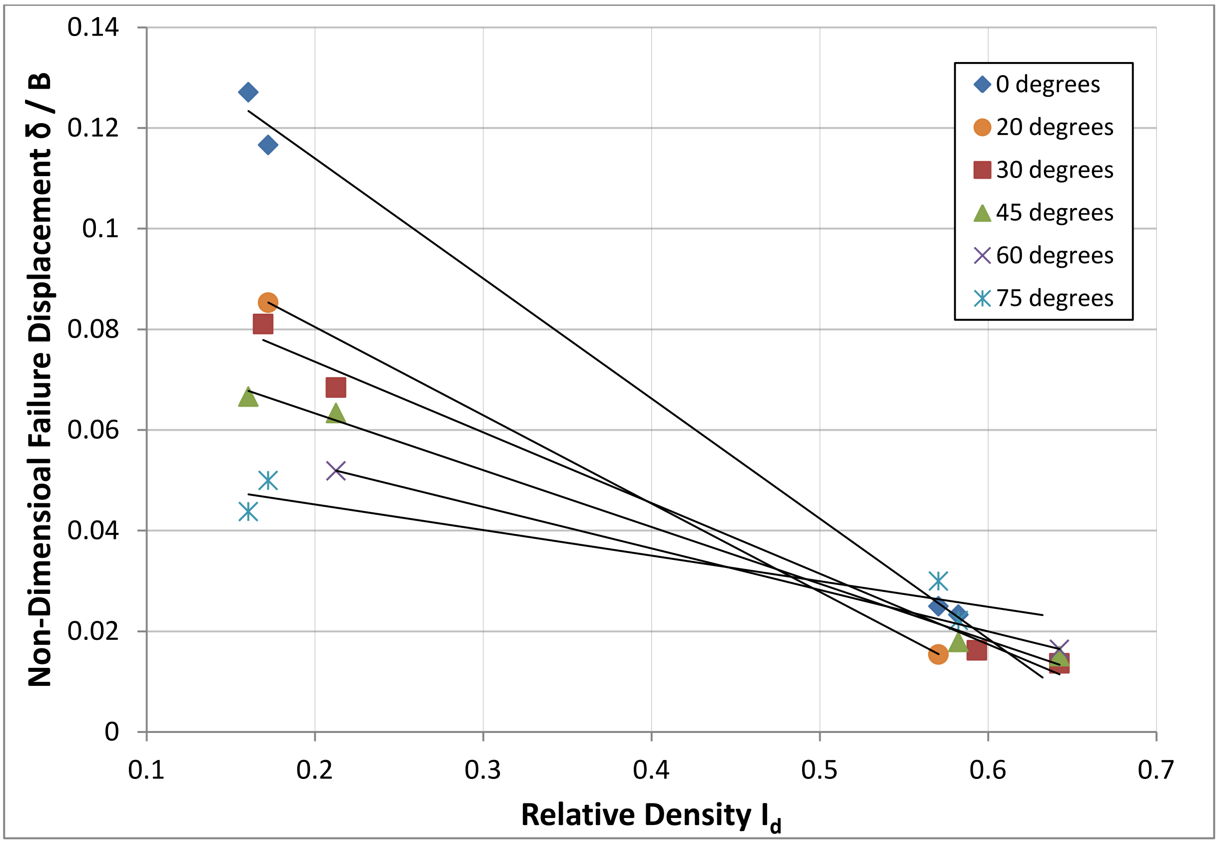


**Figure 14: δ/B against $I_d$ for various under-ream angles**

Figure 14 shows a plot of non dimensional failure displacement against relative density. The failure displacement was calculated using the double tangent method for the dense sand case due to ambiguity over the true value for some of the piles with large plateau's being seen at peak strength. For loose sand, the failure point was more obvious, being when the soil was seen to reach critical state.

From the figure, it is visible that at lower relative densities, the failure displacement decreases with an increase in the pile under-ream angle. However, at higher relative densities, any relationship between the two variables is less clear. Here, the failure displacements are very small, which explains the difficulty in viewing any data trends for this case. Further testing would be needed to determine whether the relationship between failure displacement and relative density for looser sands applies to dense sands as well, or if another or indeed no trend exists at all for these higher relative densities. These results closely match those found by Hopkins (2012), although a greater range of under-ream angles were tested in this study.

### 5.1.3 Comparison between under-ream angles

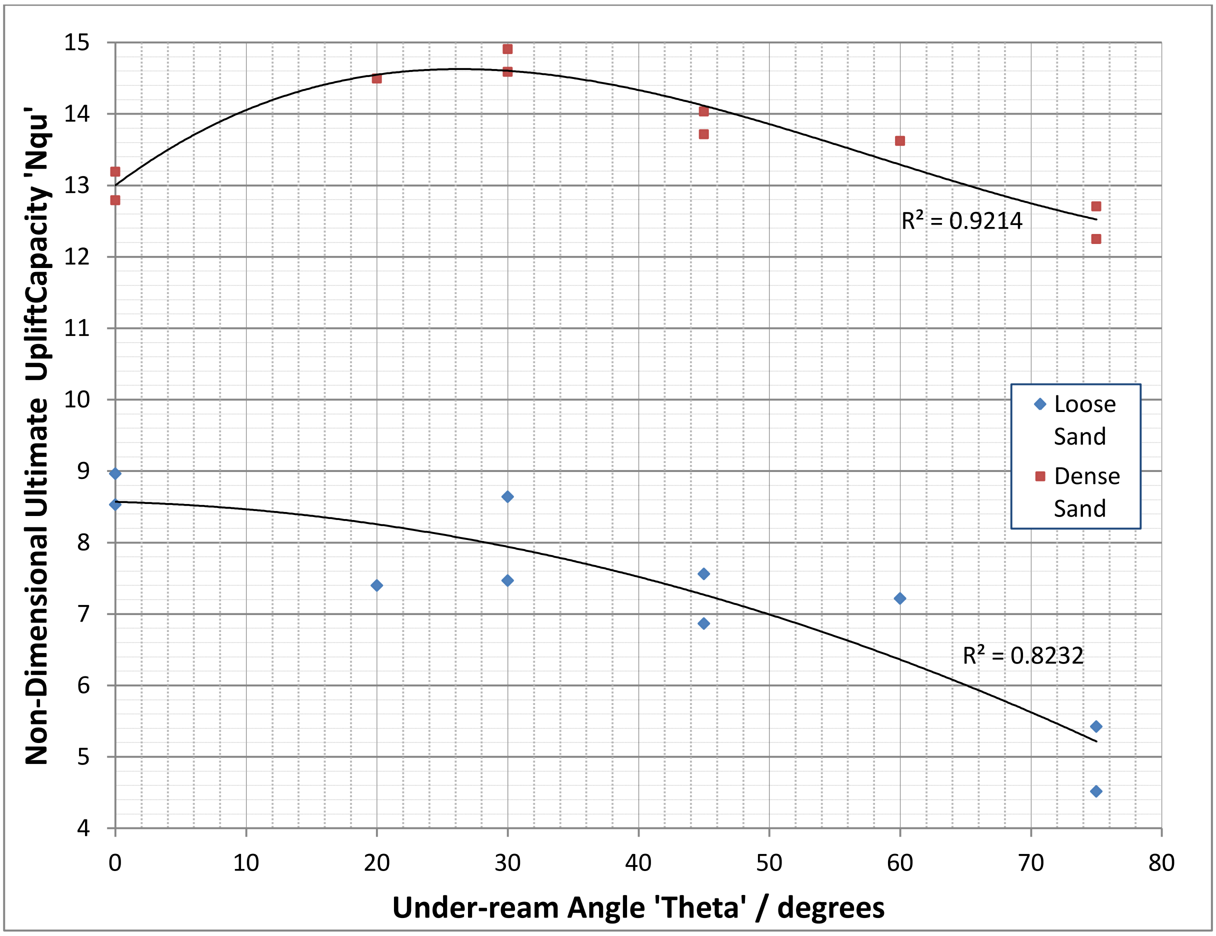


**Figure 15: Non Dimensional Ultimate uplift Capacity against under-ream angle for all pullout tests.**

Figure 15 above shows the relation between non dimensional uplift capacity $N_{qu}$ and the under-ream angle θ for all pullout tests. The average relative density was approximately 0.2 for the loose sand tests, and approximately 0.6 for the dense sand tests as shown in table 2 in section 3.10. As can be seen in figure 15, analysis of the loose sand tests yields results showing that plate anchors have the highest uplift capacity, with a drop off in strength as the under-ream angle is increased. This is especially apparent for the under-ream angle of 75°, where an approximate 40% drop in strength is noticed. This observation was also made by Hopkins (2012). This would suggest a different failure mode is occurring for the piles with high under-ream angles in loose sand. Due to the shape of the 75° pile, it is possible that a form of flow mechanism is governing here, with extensive rearrangement of the sand grains occurring instead of the soil moving upwards as a wedge. The polynomial curve fit for the loose sand results in figure 15 would also suggest that the transition to this mechanism is not instantaneous, but instead is a slower transition, given the gradually increasing uplift capacity drop off seen.

Analysis of the dense sand test results yields substantially different observations. From figure 15, the substantial degree in strength drop off for the 75 degree pile is no longer seen. In addition, an increase in uplift capacity is seen across under-reaming angles of up to around 60 degrees, which was not present in the loose sand results. This peak occurs at an angle of 26 degrees, with a magnitude of strength increase of approximately 10-15%. This under-ream angle is of particular importance because this is close to $45° – \varphi/2$ (23.5° if $\varphi$ is taken as $\varphi_{mod}$ (43°), as calculated using equations 4.15 & 4.16) which is the angle a passive failure wedge would make with the vertical when a plate is lifted up through the sand from analysis of the Mohr's circle for such a problem. Hence this result, if accurate, fits in elegantly with existing foundation theory. The peak is rather shallow in magnitude however, so in order to confirm its properties for full scale field design problems, centrifuge testing would have to be conducted to model the large scale soil stress state effectively.

## 5.2 Comparison with Theory for a Flat Plate

### 5.2.1 Load-displacement curve form

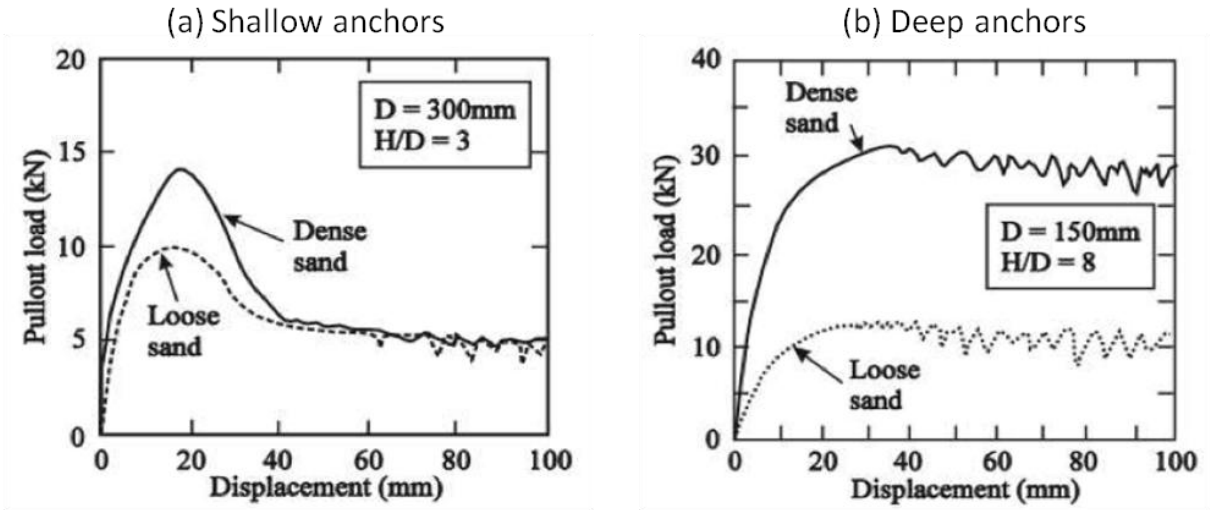


**Figure 16: Ilamparuthi et al. (2002) observed relationships between pullout load and displacement for anchors with shallow and deep embedment**

As stated in section 5.1.1, the results of Ilamparuthi et al. (2002) concerning the load-displacement relationship form did not agree with those found in this study, nor the expected behaviour of sand when subjected to a direct shear stress. Ilamparuthi et al. (2002) found that the curve form for loose and dense sands were similar at a fixed embedment, but the curve form itself changed with embedment instead of sand density as the results presented in this report and those of Hopkins (2012) show. As figure 16 shows, Ilamparuthi et al. (2002) found that shallow anchors exhibit a peak strength, with the peak for loose sand occurring at a lower displacement than dense sand, and that deep anchors show contractile behaviour up until a critical state which varies with sand density. Non dilatant behaviour such as this is not typically observed in dense sands apart from at very high confining stresses as shown in figure 17 (where $\sigma' > \sigma'_{crit}$).

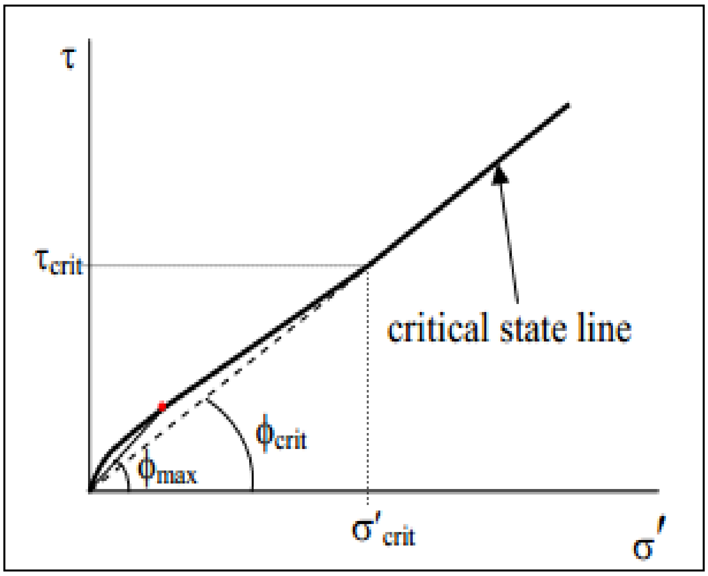


**Figure 17: Secant angle of friction for soil (CUED 3D1& 3D2 Geotechnical Databook 2012-2013)**

Although the tests of Ilamparuthi et al. (2002) were semi-large scale at 1-g, they would not have reached these sorts of stress levels due to the size of experimental rig and soil depth used, and are thus inconsistent with the expected behaviour from soil in shear and the observations in these tests. Thus, as discussed in section 5.1.1, the results from this study compare well with the expected existing theory on soil behaviour in shear, with loose sand showing contractile behaviour and dense sand showing initial dilatant strength, even if they disagree with the results of Ilamparuthi (2012).

### 5.2.2 Ultimate uplift resistance

Figure 18 shows the comparison of the experimentally determined ultimate uplift capacities against those predicted by Meyerhof and Adams (1968) for a flat plate. The black data points indicate an assumed conical failure surface, whilst the blue data points indicate an assumed cylindrical (VSSM) failure mechanism. Solid data points show data for loose sand tests and hollow points correspond to dense tests. The lines indicate when the theoretical uplift capacity equals the experimentally found capacity and 20% swings either side.

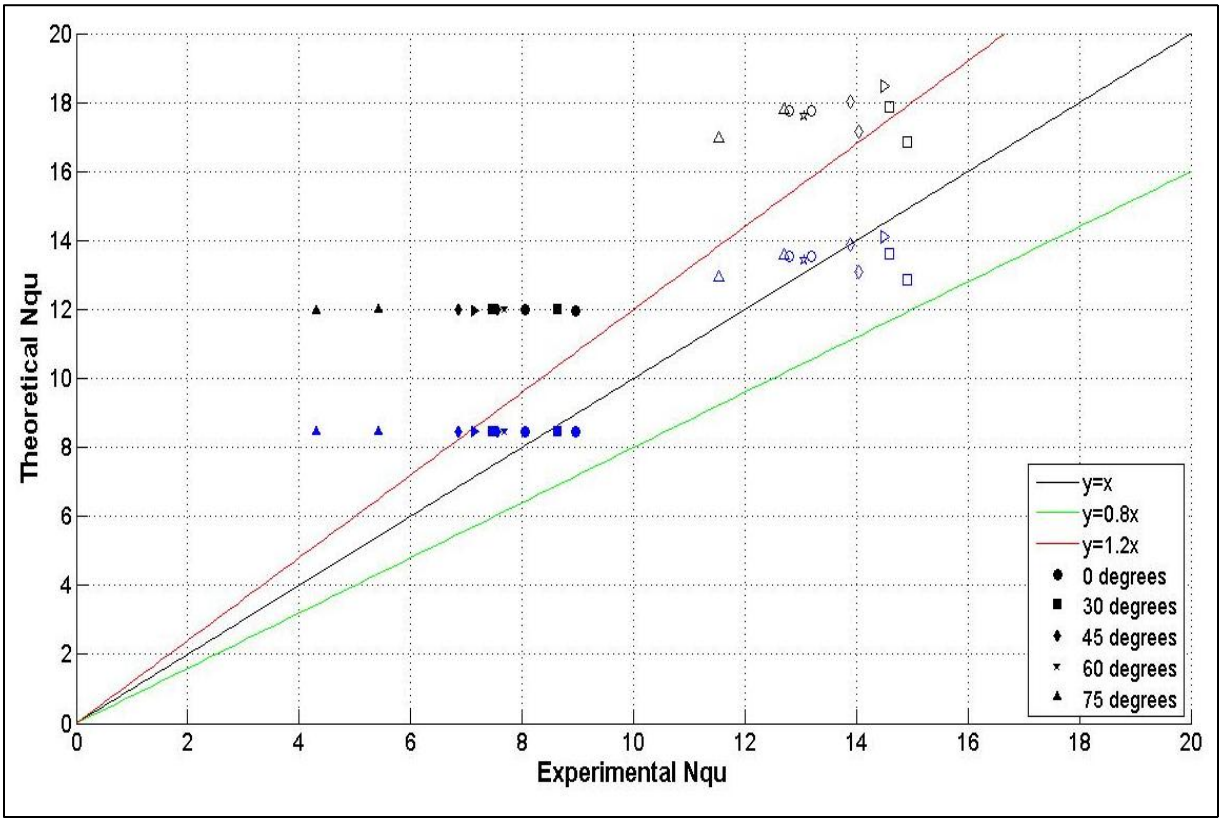


**Figure 18: Comparison of experimental ultimate uplift capacity results for all under-reamed piles to the Meyerhof & Adams (1968) theoretical for a plate anchor**

From analysis of Figure 18, we can see that when a conical failure surface is assumed, the Meyerhof theory consistently over predicts the pile uplift capacity for all sand densities tested. The 75° under-ream angle values in particular show a very large overestimate of uplift capacity, demonstrating the relation found between under-ream angle and uplift capacity detailed in section 5.1.3. It is also apparent that the model predicts the capacity to a higher degree of accuracy for denser sands than looser ones, with the denser sand points being closer on average to the y=x line and some results actually falling within 20% of the predicted values. This trend for the model being less accurate for loose sand was also observed by Geddes & Murray (1987) and Dickin (1988).

Assuming a VSSM mechanism over a conical mechanism is seen to significantly improve the Meyerhof model's accuracy from analysing figure 18. This is counter to the fact that upon pile pullout, the failure surface as observed from the soil level is not cylindrical in geometry, with the mechanisms extent at the soil surface being found to be much larger than the pile base size as shown in figure 19 and throughout section 6. Thus, as assuming a failure mechanism that is smaller in volume (and less representative of what appears to be occurring within the soil from a quick visual assessment,) appears to be more accurate from these results, this would imply that there is an inherent over-prediction in the Meyerhof model, at least for small scale tests. Via the same logic, this overestimation is likely to be within the capacity term modelling the friction on a projected soil cylinder above the pile base (outlined in section 4.1).

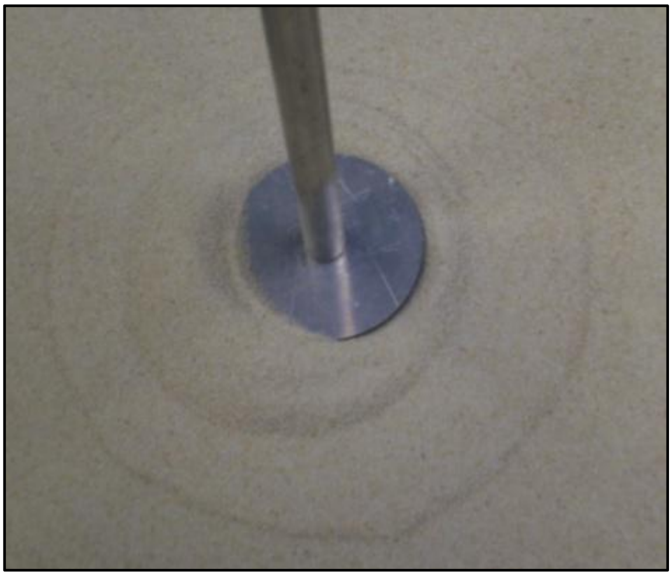

**Figure 19: Failure surface as viewed from the soil surface after pullout. It is clearly visible that the failure surface extends radially beyond the pile base and hence would suggest a non VSSM mechanism.**

### 5.2.3 Friction angle assumptions

In section 4, the modified friction angle methodology for small scale 1-g tests was described. The peak friction angle for the dense sand case using this method was calculated to be 43°. The friction angle of 46° was predicted by Bolton's stress dilatancy. Given this and the over-predictions of uplift capacity by the Meyerhof model as seen in figure 18, this implies that the modified friction angle approach does indeed improve the prediction accuracy for small scale tests, and is the sensible choice for analysis in such circumstances. Indeed, if $\varphi_{max}$ had been used instead of $\varphi_{mod}$, the predicted capacities would have been an additional 12% higher than the values displayed in figure 18.

## 5.3 Post Failure Behaviour – Soil Arching and Instability

Figure 20 highlights the oscillatory post failure soil behaviour for a 20° under-reamed pile. Similar behaviour was seen in all pullout tests and is also visible in figures 12 and 13. These oscillations were observed to continue until the pile was completely pulled out of the soil. This is caused by the phenomena of soil arching, which was observed in the half space model tests detailed in section 6. As the pile is displaced, the soil local to the under-ream forms an arch, giving the soil resistance. However, once the displacement reaches a critical value, the local soil packing becomes unstable due to the large cavity formed in the wake of the pile base. The soil local to the pile then collapses to fill this space, creating a pile load capacity drop. Afterwards, the soil is no longer unstable and the soil arch can be reformed and the process then continues to repeat itself. This behaviour was also noted by Hopkins (2012), Dickin (1988) and Oveson (1979). It was noted from comparing the processed experimental test data (examples are shown in figures12 and 13 in section 5.1) that the displacement at which this behaviour is initiated seems independent of the sand density. In addition, although such behaviour was observed to initiate at much greater displacements for the plate anchor than any of the other pile geometries tested. However, any trend further than this was not seen, with this instability being observed to initiate at approximately the same displacement for all non-zero under-ream angles tested.

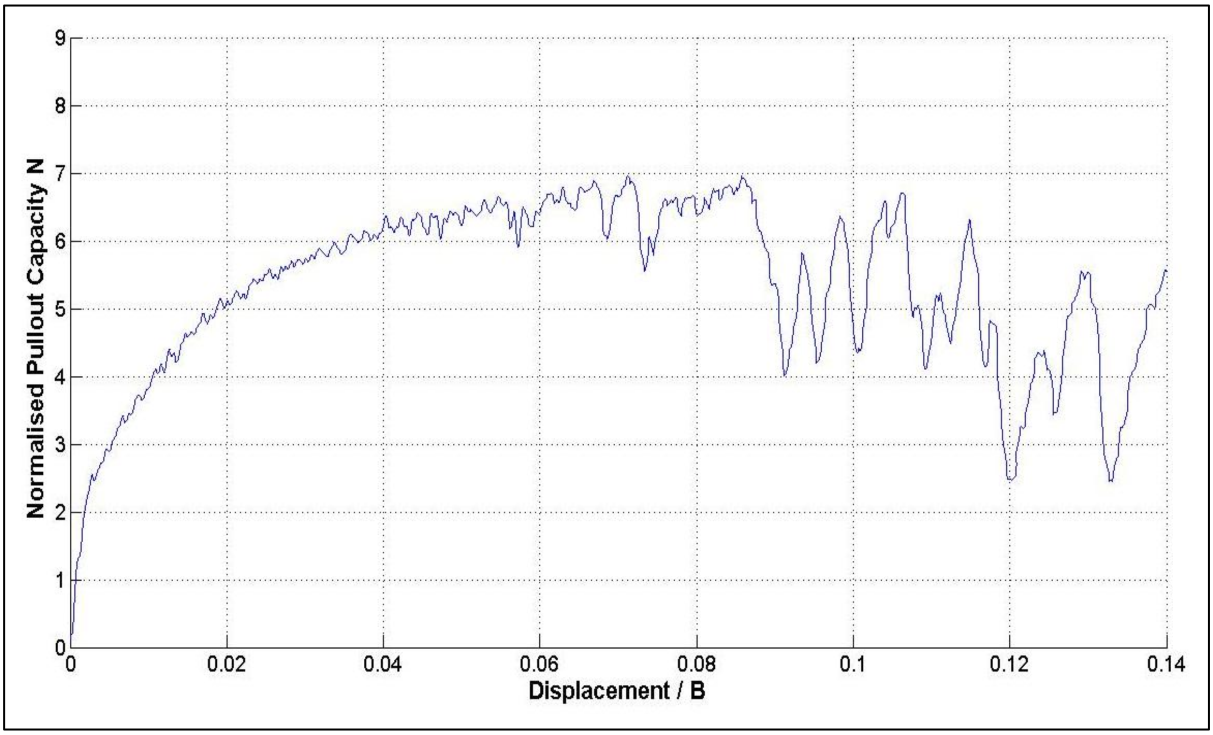


**Figure 20: Plot highlighting the post failure instability for an under-reaming angle of 20° in loose sand.**

# 6 Failure Mechanism Characterisation & Variation

This section details the results from the PIV tests, examining the failure mechanism of plate anchor and 45 degree under-ream pile models in both loose and dense sands. A Matlab script was written and used to remove all null vectors (i.e. soil regions that do not move during the experiment) to provide the figures provided in this report. The effect of varying the under-ream angle upon the mechanism geometry is deduced and discussed. The results are then compared to the existing theory for plate anchors to check the validity of approximating under-reamed piles as a plate anchor. Adjustments to the Meyerhof & Adams (1968) uplift capacity predictions are then made to represent the observed mechanism to briefly assess the Meyerhof uplift resistance model.

## 6.1 Plate Anchor

Presented here are the observed failure mechanisms for an anchor plate in both loose and dense sand. As both tests here are classified as shallow anchors by Meyerhof & Adams (1968), the expected mechanism is a truncated soil cone, extending to the soil surface. The expected angle of inclination (denoted 'Θ' – measured to the vertical) is expected to be approximately φ/2 with variation according to Ilamparuthi et al (2002) of ±2° either side, depending on the soil density.

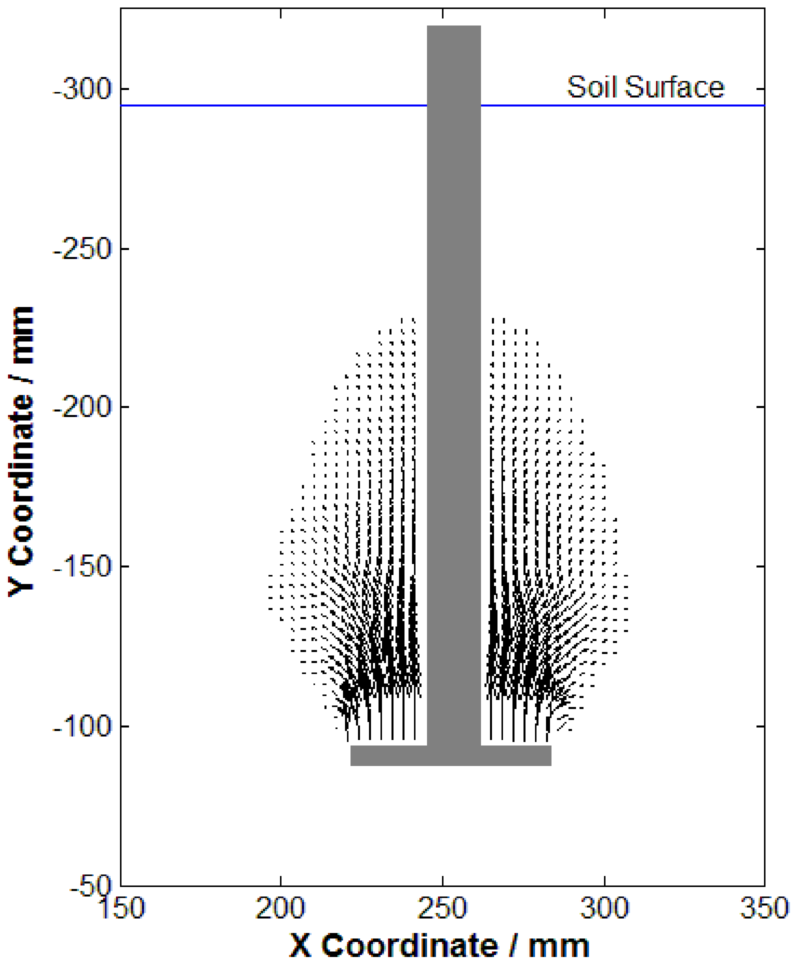


Figure 21: PIV plot of the observed failure mechanism for a plate anchor in loose sand

### 6.1.1 Loose sand mechanism

Figure 21 shows the vectoral diagram output from the PIV analysis of the loose sand mechanism for the anchor plate tested. The figure shows the pile behaving as a deep pile, with a "balloon shaped" mechanism extending approximately 125mm above the base (the embedment in this test was 200mm from table 2b) being observed. The soil movement vectors immediately above the plate anchor base are vertical. A large degree of soil contraction is observed; with the vector magnitude decreasing substantially the further the soil is from the pile base, especially in the region vertically above the base area. Some inclination of the soil vectors is seen, particularly towards the mechanism edges, with a bulge being visible immediately above the pile base where the soil is moving outward.

### 6.1.2 Dense sand mechanism

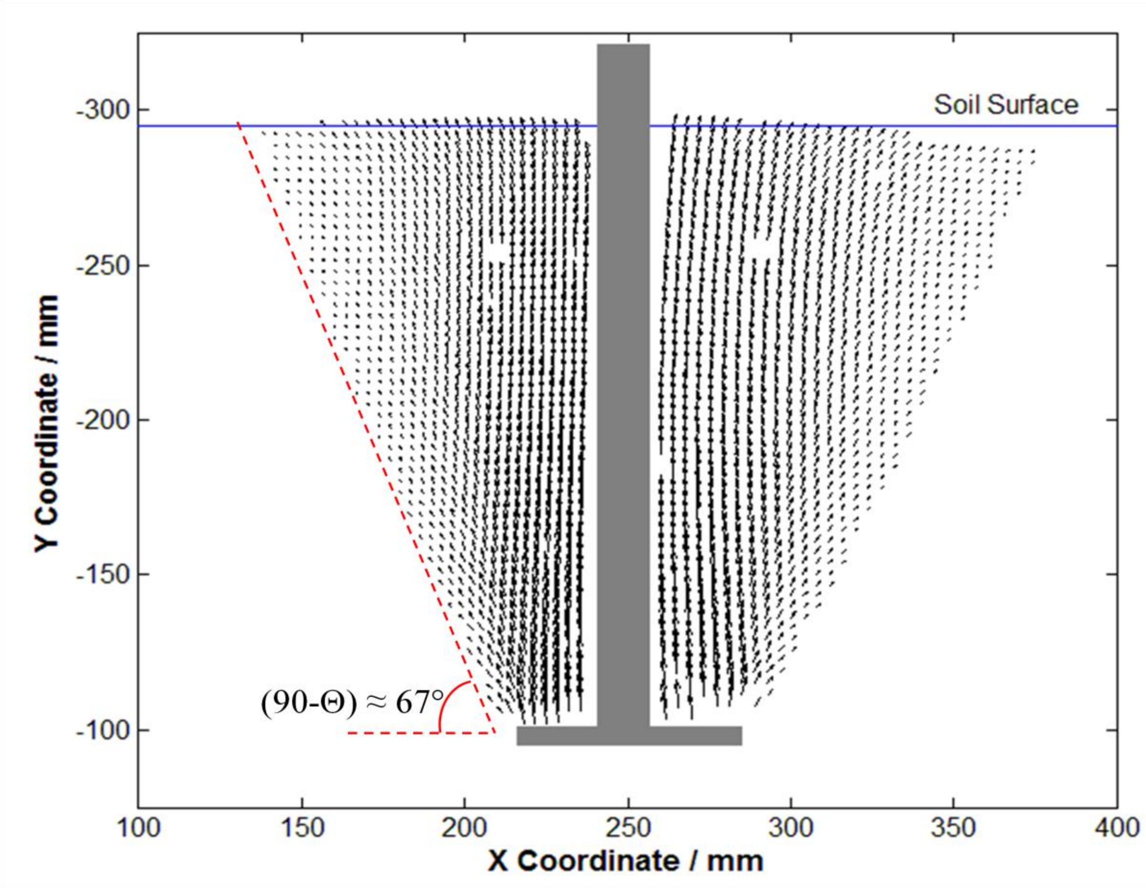


**Figure 22: PIV plot of the observed failure mechanism for a plate anchor in dense sand**

Figure 22 shows the vectoral diagram output from the PIV analysis of the dense sand mechanism for the anchor plate tested. The figure shows a conical failure mechanism extending to the soil surface level with an average angle of inclination measured to be approximately 23°. The soil in the region vertically above the base area is seen to move as a rigid block, with very little soil contraction being observed from the variation in vector magnitude up this soil column. The latter is expected because dense sand is expected to behave in a dilatant manner upon shearing, with the dense local packing limiting further compaction. The soil outside of this column also shows very little soil contraction, but is seen to displace by a smaller magnitude and at an incline, forming the soil cone observed. Lastly, as seen in the loose sand mechanism, the vectors directly above the pile base are seen to be vertical away from the base corners.

### 6.1.3 Comparison with existing theory

The dense sand mechanism described in 6.1.2 closely mirrors that found by Ilamparuthi et al. (2002) and matches the general form expected from other existing literature sources. The truncated soil cone extending to the soil surface matches the observations by Ilamparuthi et al. (2002) and the shallow anchor definition by Meyerhof & Adams (1968) well. Given that $\varphi_{mod}$ was calculated to be 43° using the methodology described in section 4.2, the average angle of inclination for the conical mechanism predicted by Ilamparuthi et al (2002) in the case for dense sand is 23.5°, but can be lower by up to 2° depending on the exact relative density of the sand. From 6.1.2, the value of 23° matches this prediction to a high degree.

However, the loose sand mechanism observed in the tests conducted here shows major differences to the predicted truncated soil cone model throughout the existing literature. The vertical extent of the failure mechanism not reaching the surface shows that in very loose sands (as tested here), the uplift force the anchor imposes on the soil is unable to be transmitted to the surface. Instead, the soil grains above the pile are rearranging and filling the available void space within the failure mechanism region, preventing chains of soil grains from effectively locking together in a manner that would enable the uplift force to be transferred across greater vertical distances. This observation matches the contractile behaviour of loose sand upon shearing expected from basic soil mechanics but contradicts the critical embedments proposed by Meyerhof & Adams (1968) (values provided in table 3, section 4.1) and the overall mechanism geometry observed by Ilamparuthi et al. (2002). The fact that the pile behaved in a shallow manner in dense sand, but in a deep manner in loose sand implies that the Meyerhof's critical embedments may vary with sand density, although further testing would be needed to confirm this.

## 6.2 Under-Reamed Base (45 degrees)

Presented here are the observed failure mechanisms for a 45° under-reamed pile in both loose and dense sand. As detailed in the literature review, next to no research has been done in this specific area. However, the work of Hopkins (2012) and the results detailed throughout section 5 in this report indicate a relationship between the base under-reaming angle and the load characteristics of the pile. This would therefore imply a change in the failure mechanism relative to the plate anchor case is occurring due to the change in under-ream angle.

### 6.2.1 Loose sand mechanism

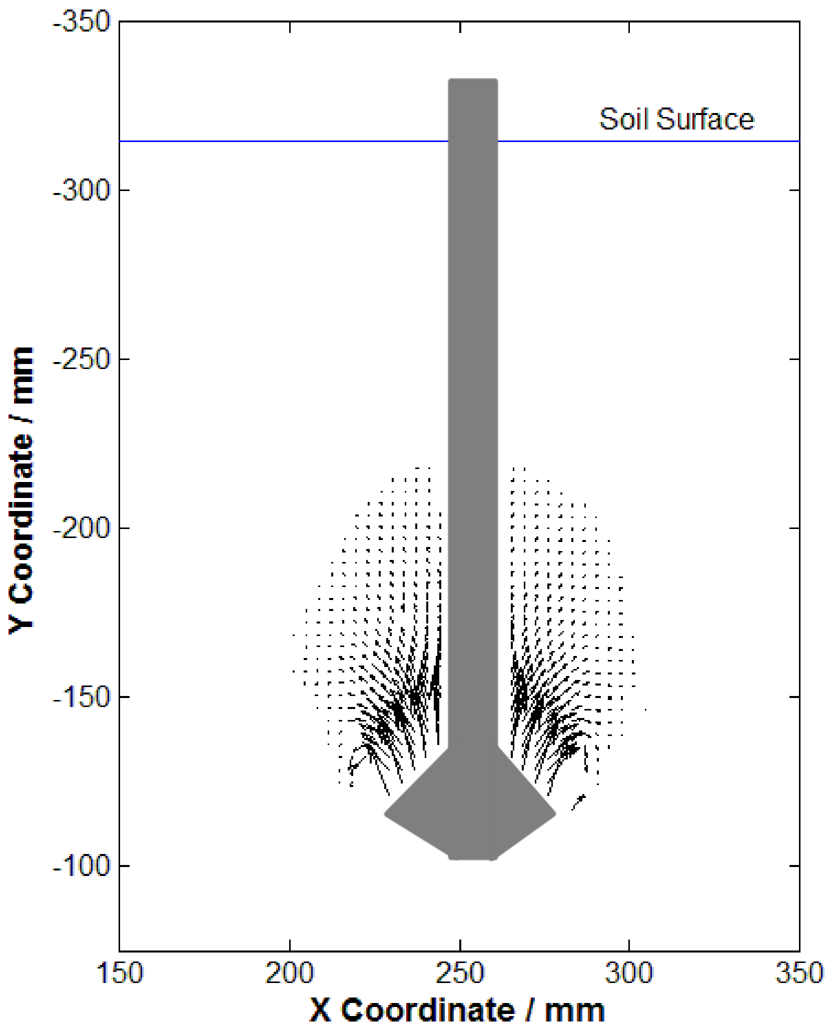


**Figure 23: PIV plot of the observed failure mechanism for a 45° under-reamed pile in loose sand**

Figure 23 shows the vectoral diagram output from the PIV analysis of the dense sand mechanism for the 45° under-reamed pile tested. The figure shows the pile behaving as a deep pile, with a "balloon shaped" mechanism extending approximately 95mm above the base (the embedment in this test was 195mm from table 2b) being observed. The soil movement vectors immediately above the plate anchor base are not vertical, with an average inclination of approximately 12° to the vertical being observed, indicating that the soil is moving upwards and outwards. As with the loose sand plate anchor mechanism, a large degree of soil contraction is observed; with the vector magnitude decreasing substantially the further the soil is from the pile base.

### 6.2.2 Dense sand mechanism

Figure 24 shows the vectoral diagram output from the PIV analysis of the dense sand mechanism for the 45° under-reamed pile tested. The figure shows a mostly conical failure mechanism extending to the soil surface level with an average angle of inclination measured to be approximately 22°, but the soil zone nearer to the base at the mechanism edge shows significant divergence from this geometry. This region is denoted as "Region X" in figure 24.

The soil in the region vertically above the base area is seen to move almost as a rigid block, with very little soil contraction being observed from the variation in vector magnitude up this soil column as expected. The soil outside of this column also shows very little soil contraction, but is seen to displace by a smaller magnitude and at an incline, forming the soil cone observed.

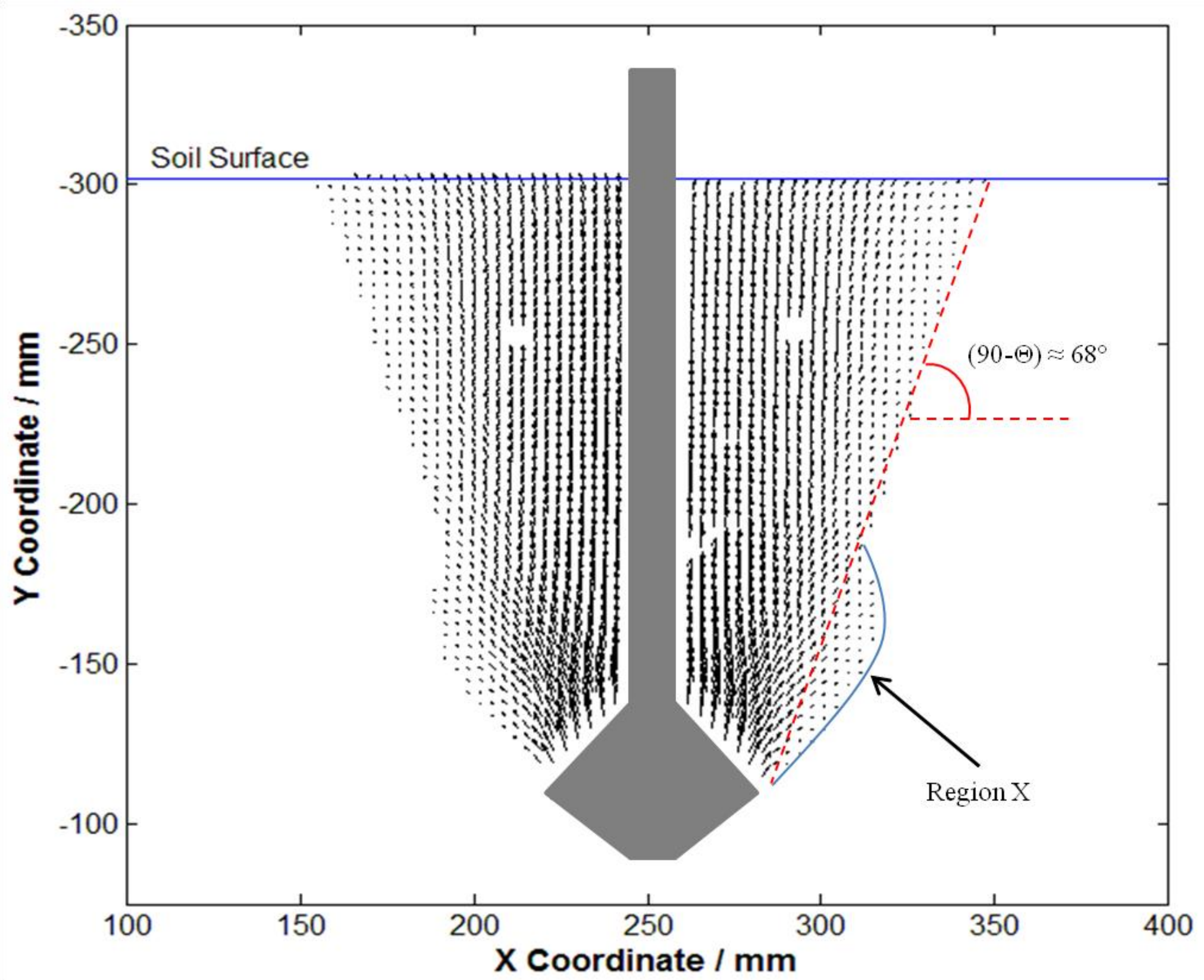


**Figure 24: PIV plot of the observed failure mechanism for a 45° under-reamed pile in dense sand**

As for the loose sand case, the soil movement vectors immediately above the plate anchor base are not vertical, with an average inclination of approximately 8° to the vertical being observed, indicating that the soil is moving upwards and outwards. This is slightly less than for the loose sand case. In the soil region local to the pile base, a small, but noticeable divergence away from the conical geometry is visible, with a curved slip surface being observed.

### 6.2.3 Comparison to plate anchor theory and results

Both figures 23 and 24 indicate that the variation in under-ream angle does alter the uplift failure mechanism when compared with figures 21 and 22. Both mechanisms show an alteration in the direction of soil movement directly on top of the pile base. However, the inclination angle found was much smaller than the change in under-ream angle (i.e. 45°) between the two cases. In this study, only smooth aluminium piles were tested, and as such, the low value of soil-pile interface friction angle (δ) may be the cause for this smaller than expected rotation of soil movement. However, without further study, the reasoning behind this observation cannot be concluded with certainty, but its presence can be. The presence of this phenomenon across both sand density specification only reinforces this.

For the dense failure mechanism, the divergence from the soil cone geometry in the region closer to the pile base noted in 6.2.2 (Region X) can be described as a "hemisphere of expansion". The soil in this more circular region of the mechanism, i.e. where it is closer to the enlarged section of the pile base, is seen to be experiencing a combination of uplift and form of cavity expansion based on the geometry observed, whilst soil significantly above / far away from the pile base level does not experience this effect and follows the conical mechanism expect for the plate anchor case. This local change in the failure mechanism geometry not only increases the weight of the soil mass that is lifted, but also increases the length of the shear bands present and hence explains the small, but noticeable increase in uplift capacity noted in section 5.1.3. Similarly, for the loose sand case, the mechanism has been shown to decrease in effective volume and surface area from the results presented in sections 6.1.1 and 6.2.1. Thus, because the weight of the lifted soil mass is decreased and the area of the mechanism shear band is also lowered, the capacity decrease observed in section 5.1.3 for the 45° under-ream relative to the plate anchor case is explained.

Thus in summary, variation in the under-ream angle is seen to have an impact of the failure mechanism geometry, which logically explains the uplift capacity trends observed throughout the testing in this study. However, it should be noted that only 2 pile geometries were tested due to the time constraints associated with 4$^{th}$ year projects, and so to fully validate this conclusion, more specimens with a wider variety of under-ream angle should be tested.

## 6.3 Meyerhof Evaluation & Adjustments Based on the True Failure Mechanism

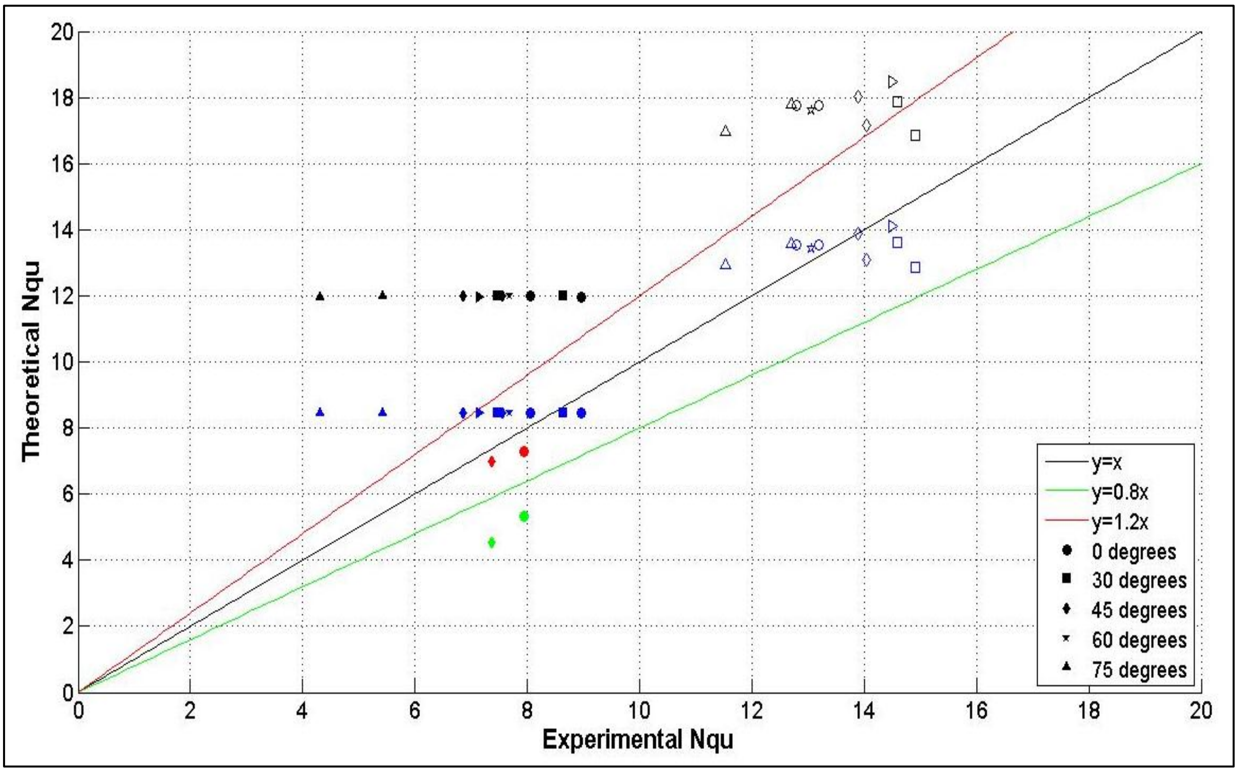


**Figure 25: Comparison of experimental ultimate uplift capacity results against the Meyerhof & Adams (1968) theoretical predictions for a plate anchor. The red and green data points represent the adjusted loose sand mechanism, with red maintaining the Meyerhof classification of a shallow anchor, and the green using the deep pile calculation.**

The red and green points in figure 25 show the predicted capacities when adjusted using the observed mechanism. The red points indicate where only the "weight of soil mass lifted" term has been adjusted, maintaining the shallow anchor behavioural assumption as predicted via the critical embedment depths proposed by Meyerhof & Adams (1968) presented in section 4.1. The green points use the formulae for deep plate anchors and so adjust both terms in the Meyerhof formulae. The soil weight term adjustment was carried out using volumetric integrals of the mechanism geometry shown in figures 21 and 23.

First consider the loose sand results. As is clearly visible from figure 25, using the observed loose sand mechanism in Meyerhof's model creates a conservative result. The result can also be seen to be more conservative if the critical embedment depth values are ignored and the type of mechanism (shallow or deep), is treated as an exogenous variable as opposed to an endogenous variable dependant on the soil friction angle. Because we can see that the assumed mechanism form used by Meyerhof & Adams (1968) (a conical shape or something of similar form) was wrong, the shape factors to convert from the strip footing case to the fully 3d case may no longer be accurate. This would potentially explain the inaccuracy, although further testing would be needed to confirm whether this is the case and if so, what form the adjustment should take. For the moment however, the shape factors may be adjusted using the following formula:

$$Adjusted\ Shape\ Factor\ s' = k\left(1 + \frac{mH}{D}\right) = ks \tag{7.1}$$

where k is a constant to correct the theoretical capacity predictions. From the tests conducted, k values for the plate anchor and 45 degree pile have been computed for use with the deep embedment formula (the pile was observed to behave in that manner) and presented below in table 5. Further testing at both large and small scales is required to validate this approach.

**Table 5: Adjusted shape factors to correct the Meyerhof & Adams (1968) uplift capcity predictions for the loose sand case.**

| Pile Under-ream Angle | 0° | 45° |
|---|---|---|
| k | 1.52 | 1.67 |

Now considering the dense sand case separately, from figures 22 and 24, we can see that the Meyerhof critical embedment depths correctly predict the behavioural category of the pile. Thus the black data points on figure 25 (plotted assuming the Ilamparuthi et al. (2002) truncated soil cone model) represent the Meyerhof predictions when the true, observed mechanism is used. As noted in section 5.2.2, assuming a VSSM (i.e. a mechanism of smaller volume and shear band length) has been seen to improve the Meyerhof predictions for these tests results. Hence, for dense sand, because the weight of the lifted soil mass term has been observed to be accurate, there must be an overestimation of the frictional term in Meyerhof's formula (equation 4.8).

From the derivation in section 4 and Meyerhof & Adams (1968), this term is derived assuming that the frictional resistance caused by the soil is localised at the interface between a central cylinder of soil above the anchor base, which moves up as a rigid block, and the soil zone in-between this and the actual mechanism edge. From figures 22 and 24 however, the transition between this central soil cylinder and the rest of the mechanism is gradual in nature, with this localisation not being observed. Thus, this would imply that the assumption in deriving this frictional term is not valid, at least for small scale tests. Given the greater amount of empirical evidence (as discussed in the literature review) claiming good agreement with Meyerhof's predictions at the larger scale, especially for piles behaving in a shallow manner, centrifuge or full scale testing would be advised to check whether this conclusion is only applicable for small scale testing regimes.

# 7 Conclusions and Recommendations for Future Work

## 7.1 Performance of Piles

From the tests conducted for this project, it is possible to conclude that increasing the sand density increases the uplift capacity and lowers the pile displacement at which failure occurs. The load-displacement curve shapes were shown to follow those seen on simple shear box soil tests, with a dilatant peak strength being seen for sense sands and contractile behaviour for loose sands, with both tending towards a critical state at large displacements.

Post failure oscillatory instability was observed to commence at large displacements for all under-ream angles. It can be concluded that this phenomena initiates at significantly large displacements for the plate anchor case than any of the non zero under-ream angle values tested. Beyond this however, data trends are less clear, with the difficulty in defining exactly when this instability initiates and the closeness of initiation for differing under-ream angles limiting further conclusions at this stage.

The theoretical model proposed by Meyerhof & Adams (1968) was evaluated against the experimental data from this report. In both loose and dense sands, assuming the truncated cone mechanism, the theoretical predictions of the model were significantly above the observed experimental capacities, with an overestimate upwards of 20% being seen. The predictions for the dense sand case were more accurate than for the loose sand case. However, if a VSSM was used, the predictions were significantly more accurate, predicting the plate anchor capacities very closely in both loose and dense sand cases.

In both loose and dense sands, the under-reaming angle was observed to have an influence on the uplift capacity of the pile, with differing relationship forms for each case. For loose sands, the plate anchor was observed to exhibit the highest uplift capacity, with a progressive capacity drop off as the under-reamed angle was increased. At large angles (around 75 degrees), this drop off was significant, with a strength decrease of approximately 40% relative to the plate anchor case being detected. In contrast, for dense sand, the relationship between uplift capacity and under-reaming angle showed a peak strength occurring at an angle of approximately 25 degrees. Although this angle is close to the angle of a passive soil wedge at failure ($45° - \varphi/2$), more data would be advised to confirm this. Hence, further work is advised to investigate this. The capacity increase observed was 10-15%, with the strength drop off at large under-reaming angles being less severe than as observed for loose sands.

## 7.2 Failure Mechanism Characterisation

From the half space model tests, the failure mechanism for a plate anchor in dense sand was shown to closely match the truncated cone mechanism highlighted in Ilamparuthi et al. (2002), with an average inclination angle of $\varphi/2$. However, the observed mechanism for loose sand in these tests failed to reach the soil surface. Similar behaviour was observed for the 45 degree under-ream. This would imply that either under-reamed piles in very loose sands can behave as deep piles, even when their embedments are lower than the critical values proposed by Meyerhof & Adams (1968) or the critical embedment values are a function of relative density although not original implied so. Further investigation would be required to identify which is the case.

From the PIV test on the 45° under-ream, the under-reaming angle was observed to alter the mechanism from the plate anchor case. Local to the pile base, the sand vectors were shown to rotate from the vertical by 12° for loose sand, and 8° for dense sand. These values are much smaller than the 45° under-ream and the rotation expected. A possible reason for this was identified as being due to the smooth aluminium alloy the model piles were manufactured from, resulting in a low soil-pile interface friction angle. In loose sand, the vertical extent of the failure mechanism dropped significantly from the pate anchor case, explaining the capacity drop observed in the pullout tests. In dense sand, a conical mechanism similar to the plate anchor was observed, but with an added zone of soil movement near the pile base. This added zone is curved in nature, implying soil local to the pile is experiencing some manner of cavity expansion combined with the standard uplift mechanism, although further investigation is advised as only 2 pile geometries were tested for this project due to time constraints. This additional zone, if consistent over further testing, would validate the increase in capacity seen for piles in dense sand seen in sections 5 and 7.1.

Using the observed failure mechanism, adjustments to the weight of the lifted soil mass term for the loose sand case were made using approximate volumetric integrals to compare these adjusted predictions to predictions of Meyerhof & Adams (1968). The new theoretical predictions showed discrepancy to the experimental observations but were conservative when the observed mechanism geometry was used. Due to the extensive differences between the observed mechanisms geometry and that assumed by Meyerhof & Adams (1968) revised shape factors were calculated to correct the predictions, but further work is advised to determine and correct this discrepancy between the model and reality for loose sands. For dense sands, the over-prediction of uplift capacity for the observed mechanism geometry was found to be present in the equation term modelling the soils frictional resistance. A potential reason for this was proposed, being that Meyerhof's approximation of the frictional force being localised onto a cylindrical surface projected above the pile base was inaccurate, or over simplified.

## 7.3 Future Work

### 7.3.1 Small scale modelling

This project has made headway into the investigation of under-reamed pile behaviour, but the problem is far from completely understood. Following on from Hopkins (2012), this project has involved testing at the 1-g level, with both fully formed models and half space models for characterising the failure mechanism. If further 1-g testing is to be conducted (especially on the under-reamed case where test data is sparse), future recommended testing would include:

- Experiments using greater embedment depths to measure the deep pile response, especially in dense sand stratum, with possible investigation into the critical embedment depth values proposed by Meyerhof & Adams (1968).
- A comparison study between rough and smooth piles would be useful, particularly with half space models to view its influence on the uplift failure mechanism.
- Testing in layered sand stratum would also be recommended, due to the lack of experimental studies in this region whilst investigating the influence of loose or dense overlying stratum relative to the layer the pile base is embedded in. Both pullout tests of fully formed piles and PIV tests using half space models would be advised.
- A greater range of pile base diameter's and sand densities tested, to better fill out the data set available.
- Further PIV tests on a greater range of under-reams, to get a more complete picture of the effect varying the under-ream angle has upon the failure mechanism geometry. Particular focus might be allocated to large under-ream angles, where in this report and the research by Hopkins (2012) noticed a substantial drop off in uplift capacity, (at least in loose sands,) which would suggest a transition in failure mechanism form that should be investigated.
- Tests on a wider range of soil types, to better cover the range of soils encountered in nature would be highly advised. This project has considered the uplift response in dry, homogeneous sand stratum, and hence saturated sand stratum and clays of varying densities and strengths should also be tested. For such soils, the loading rate will have

to be carefully considered to provide clarity on whether a drained or undrained response is being measured. As such, pore pressure distributions should be measured for such experiments to see what impact pore pressures on the pile base have on the uplift capacity of the pile.

However, these investigations will still only be comparative in nature due to the problems testing at 1-g levels and thus large scale modelling is advised. Although such an experimental regime lowers the numbers of tests that can be conducted, the data from each one is more valuable as actual field ground conditions are better replicated in such experiments.

### 7.3.2 Large scale modelling

As previously mentioned, small scale tests at 1-g have problems inherent in their nature. With soil confining stress levels being much smaller than commonly experienced in the field, far larger dilation angles are expected and hence a disparity between the load-displacement between the two cases becomes apparent. Hence the ideal desired future work regime would involve centrifuge or full scale testing to confirm whether the conclusions in this report hold up under practical scenarios. As highlighted in the literature review, there is a substantial lack of centrifuge / field test data for the general under-reamed case, with past research focusing on the plate anchor case. Such data would help clarify the impact of varying the under-ream angle on a piles load response for use in practical situations. It is thus recommended to test the conclusions made in this report under such conditions, preferably using a geotechnical centrifuge as they provide numerous advantages from a research point of view. Additionally, any of the small scale investigations recommended in section 7.3.1 would also be recommended to be conducted at large scale levels.

# References

Baker, W.H., and Konder, R.L., 1966, "Pullout load capacity of circular earth anchor buried in sand", *National Academy of Sciences,* Highway Research Board, Report 108, pp. 1-10.

Balla, A., 1961, "The Resistance of Breaking out of Mushroom Foundations for Pylons", *Proceedings of the 5th International Conference on soil mechanics and Foundation Engineering,* Paris, 1:569-576.

Bolton, M., 1986, "The Strength and Dilatancy of Sand", *Geotechnique,* 36(1), pp. 65-78.

Bolton, M., White, D.J. & Cheuk, C.Y., 2008, "The uplift resistance of pipes and plate anchors buried in sand", *Geotechnique,* pp. 771-779

civil-engg-world.blogspot.co.uk, 2012, Black Cotton Soil of Deccan Lava Plateau [Online] Available at: http://civil-engg-world.blogspot.co.uk/2012/05/black-cotton-soil-of-deccan-lava.html, [Date last accessed: 13/05/2014]

CUED 3D1 & 3D2 Geotechnical Engineering Databook 2012-2013 Available online at https://camtools.cam.ac.uk/, [Date last accessed: 13/05/2014]

Davies, E.H., 1968, "Theories of plasticity and the failure of soil masses", In: *Soil Mechanics: Selected Topics,* London: Butterworth's, pp. 341-380.

Dickin, E.A., 1988, "Uplift behaviour of horizontal anchor plates in sand", *Journal of Geotechnical Engineering,* ASCE, 114(1): 1300-1317.

Drescher, A. & Detourney, E., 1993, "Limit Load in translational failure mechanisms for associative and non associative materials", *Geotechnique,* 43(3), pp. 443-456.

Flavigny, E., Desrues, J. & Palayer, B., 1990, Note Technique - Le Sable d'Hostun "RF". *Revue Francaise de Geotechnique,* pp. 67-70.

Haskell, J.J.M., 2013, *Guidance for the design of pile groups in laterally spreading soil,* s.l.: Cambridge University: PhD thesis.

Hopkins, A., 2012, *The Uplift Capacity of Under-Reamed Piles,* s.l.: CUED: fourth year undergraduate project report.

Ilamparuthi, K., Dickin, E.A. & Muthukrisnaiah, K., 2002, "Experimental investigation of the uplift behaviour of circular plate anchors embedded in sand", *Canadian Geotechnical Journal,* pp. 648-664.

Khadilkar, B.S., Paradkar, A.K. & Golait, Y.S., 1971, "Study of rupture surface and ultimate resistance of anchor foundations", *Proceedings of the 4th Asian Regional Conference on Soil Mechanics and Foundation Engineering, Bangkok, Thailand,* Vol. 1, pp. 121-127.

Merifield, R.S. & Sloan, S.W., 2006, "The ultimate pullout capacity of anchors in frictional soils", *Canadian Geotechnical Journal,* 43(8), pp. 852-868.

Meyerhof, G.G. & Adams, J.I., 1968, "The ultimate uplift capacity of foundations", *Canadian Geotechnical Journal,* 43(8), pp. 225-244.

Mitrani, H., 2006. *Liquefaction Remediation Techniques for Existing Buildings,* s.l.: Cambridge University: PhD thesis.

Oveson, N.K., 1979, "The use of physical models in design: the scaling law relationship", *Proceedings of the 7th European Conference on Soil Mechanics & Foundation Engineering, Stockholm, Sweden,* Vol. I, pp. 717-722.

Schanz, T. & Vermeer, P.A., 1996, "Angles of friction and dilatancy of sand", *Geotechnique,* 46(1), pp. 145-151.

# APPENDIX – Risk Assessment Retrospective

Due to the experimental nature of the project, a full risk assessment was undertaken, in addition to the mandatory Schofield Centre induction. Specific hazards identified before the experiments were undertaken as a part of the risk assessment were:

- Dust Hazard – When pouring sand, dust was typically given off which if inhaled, could cause respiratory issues. The control measure implemented was to use one of the designated respirator masks provided by the Schofield Centre whenever sand was being poured. In addition, the room where pouring took place was sealed and dust extractors were used.
- Heavy Lifting – Sand bags weighing upwards of 25kg and heavy experimental equipment had to be lifted and moved throughout the experimental preparatory procedure. Correct lifting procedures were employed, and any equipment deemed unsafe to carry alone was either moved using a pallet truck, or with the help of another individual. No injuries were sustained from lifting objects in this project.
- Use of the actuator and electrical equipment – the 1D actuator used had multiple moving parts and weighed a substantial amount. The control measures implemented were to only physically handle the actuator when the power supply was turned off, and to control it remotely during experiments. In addition, all electrical equipment was handled with due safety precautions.
- Transportation of the test container – In order to manoeuvre the pullout test tub to the vibrating table, it was transported via the use of a forklift truck. This was done by a trained Schofield Centre operator at all times. No problems were encountered transporting the test container.

This risk assessment conducted reflected the hazards actually encountered in the project to a very high degree, with all significant hazards being identified before the experiments were undertaken. No injuries were sustained throughout the projects experimental work, in part because of the thorough risk assessment undertaken at the projects commencement. Because of the thorough and adequate nature of the risk assessment conducted, if I were to start the project again, I would assess risk in the same manner.